

# Can acoustic and axion-like early dark energy still resolve the Hubble tension?

Théo Simon<sup>1,\*</sup>

<sup>1</sup>*Laboratoire Univers & Particules de Montpellier (LUPM),  
CNRS & Université de Montpellier (UMR-5299),  
Place Eugène Bataillon, F-34095 Montpellier Cedex 05, France*

In this paper, we reassess the ability of the acoustic early dark energy (ADE) and axion-like early dark energy (EDE) models to resolve the Hubble tension in light of the new Pantheon+ and  $SH_0ES$  data on the one hand, and the BOSS LRG and eBOSS QSO data, analyzed under the effective field theory of large-scale structures (EFTofLSS) on the other hand. We find that the Pantheon+ data, which favor a larger  $\Omega_m$  value than the Pantheon data, have a strong constraining power on the ADE model, while the EFTofLSS analysis of the BOSS and eBOSS data only slightly increases the constraints. We establish that the ADE model is now strongly disfavored as a solution to the Hubble tension, with a remaining tension of  $3.6\sigma$  (according to the  $Q_{\text{DMAP}}$  metric). In addition, we find that the axion-like EDE model performs better when confronted to the same datasets, with a residual tension of  $2.5\sigma$ . This work shows that the Pantheon+ data can have a decisive impact on models which aim to resolve the Hubble tension.

## I. INTRODUCTION

The  $\Lambda$  cold dark matter ( $\Lambda$ CDM) model provides a remarkable description of a wide variety of data from the early universe – such as cosmic microwave background (CMB) or big bang nucleosynthesis (BBN) –, as well as observations of large scale structure (LSS) from the late universe – including the baryon acoustic oscillation (BAO) and the uncalibrated luminosity distance to supernovae of type Ia (SNIa). However, as the accuracy of cosmological observations has improved, the concordance cosmological model starts showing several experimental discrepancies. Among them, the Hubble tension refers to the inconsistency between local measurements of the current expansion rate of the Universe, quantified by the Hubble constant  $H_0$ , and the values inferred from early universe data assuming the  $\Lambda$ CDM model. More precisely, this tension is essentially driven by the *Planck* Collaboration’s observation of the CMB, which predicts a value of  $H_0 = 67.27 \pm 0.60$  km/s/Mpc [1] within the  $\Lambda$ CDM model, and the value measured by the  $SH_0ES$  Collaboration using the Cepheid-calibrated cosmic distance ladder, whose latest measurement yields  $H_0 = 73.04 \pm 1.04$  km/s/Mpc [2, 3]. The disagreement between these observations results in an  $\sim 5\sigma$  tension. Experimental efforts are under way to establish whether this discrepancy can be caused by systematic effects (see, *e.g.*, [4–9]), but no definitive explanation has yet been found. This tension could therefore be indicative of new physics, most likely located in the pre-recombination era, which involves a reduction in the sound horizon before recombination [10–15]. Early dark energy (EDE) models are capable of producing such an effect by increasing the total energy density of the Universe before recombination with the addition of a scalar field [16–37] (for review of EDE models see Ref. [38], and for a review of models

that could resolve the Hubble tension see Refs. [15, 39]). In the following, we consider the specific case of acoustic dark energy (ADE) developed in Refs. [40, 41].

In this paper, we reassess the constraints on the ADE and axion-like EDE models (paying particular attention to the former) and their ability to resolve the Hubble tension, by successively evaluating the impact of the effective field theory (EFT) full-shape analysis applied to the BOSS LRG [42] and eBOSS QSO [43] data, and the impact of the Pantheon+ data [44]. On the one hand, we make use of developments of the one-loop prediction of the galaxy power spectrum in redshift space from the effective field theory of large-scale structures (EFTofLSS)<sup>1</sup> applied to the BOSS [64] and eBOSS [65] data in order to constrain the ADE and axion-like EDE models. This novel theoretical framework has made it possible to determine the  $\Lambda$ CDM parameters at precision higher than that from conventional BAO and redshift space distortions analyses, and even comparable to that of CMB experiments. In addition, the EFTofLSS provides an important consistency test for the  $\Lambda$ CDM model and its underlying assumptions, while allowing one to derive competitive constraints on models beyond  $\Lambda$ CDM (see, *e.g.*, Refs. [64–83]). The study of the EFTofLSS impact on the ADE constraints is similar to what has already been done for the axion-like EDE model in Ref. [84] (see also Refs. [85–87]), which showed that this model leaves signatures in the galaxy power spectrum on large scales that can be probed by the BOSS data. On the

---

<sup>1</sup> The first formulation of the EFTofLSS was carried out in Eulerian space in Refs. [45, 46] and in Lagrangian space in [47]. Once this theoretical framework was established, many efforts were made to improve this theory and make it predictive, such as the understanding of renormalization [48, 49], the IR-resummation of the long displacement fields [50–55], and the computation of the two-loop matter power spectrum [56, 57]. Then, this theory was developed in the framework of biased tracers (such as galaxies and quasars) in Refs. [58–63].

---

\* Electronic address: theo.simon@umontpellier.fr

other hand, we update the constraints on the ADE and axion-like EDE models by considering the Pantheon+ data from Ref. [44]. It has already been shown in Ref. [84] that the combination of the Pantheon+ data with a  $SH_0ES$  prior provides better constraints on the axion-like EDE model than the equivalent analysis including Pantheon data. This can be interpreted as a consequence of the fact that the Pantheon+ data prefer a value of  $\Omega_m = 0.334 \pm 0.018$  which is higher than that of the Pantheon data. Together with the measured value of  $H_0 = 100 \cdot h$  km/s/Mpc by  $SH_0ES$ , it leads to an increased value of  $\omega_{\text{cdm}} = \Omega_{\text{cdm}} \cdot h^2$  (see Ref. [88]), which cannot be fully compensated by the presence of EDE, therefore degrading slightly the fit to CMB data.

In Sec. II, we provide a review of the ADE and axion-like EDE models, as well as a description of the analysis method and the datasets to which these models will be subjected. In Sec. III, we present the constraints of the ADE model and compare them to the axion-like EDE case, while in Sec. IV we consider some additional variations of the model under study.

## II. THE MODEL AND THE DATA

### A. Review of the ADE model

In this paper, we focus on the acoustic dark energy (ADE) model proposed in Ref. [40] (see Ref. [38] for a general introduction). In this model, the ADE equation-of-state parameter,  $w_{\text{ADE}}(a) = P_{\text{ADE}}(a)/\rho_{\text{ADE}}(a)$ , is modeled as

$$w_{\text{ADE}}(a) = \frac{1 + w_f}{[1 + (a_c/a)^{3(1+w_f)/p}]^p} - 1. \quad (1)$$

In Fig. 1, we plot the evolution of  $w_{\text{ADE}}$  as a function of the cosmological redshift  $z$ . This figure clearly illustrates that in this model the critical redshift  $z_c = (a_0 - a_c)/a_c$  sets a transition in the ADE equation-of-state from  $w_{\text{ADE}} \rightarrow -1$ , when  $z \gg z_c$ , to  $w_{\text{ADE}} \rightarrow w_f$ , when  $z \ll z_c$ . Therefore, this parametrization allows the ADE component to behave in a similar way to dark energy before the critical redshift (exactly like the axion-like EDE model), while it allows the late-time value of the ADE equation-of-state to be set thanks to the parameter  $w_f$ . As shown in Fig. 1, the rapidity of this transition is controlled by the parameter  $p$ , which is set at  $p = 1$  for our baseline model, corresponding to the modeling of the time-averaged background equation-of-state of the axion-like EDE model [89]. Similar to the axion-like EDE case where  $w_{\text{EDE}}(z \ll z_c) = 1/2$  (see below), the ADE dilutes faster than the radiation (*i.e.*,  $w_f > w_r$ ) below the critical redshift, in order to suppress the contribution of this component to the total budget of the Universe at the moment of the CMB.

Let us note that the parametrization of Eq. (1) can be achieved in the K-essence class of dark energy models. In particular, the dark component is here a perfect fluid represented by a minimally coupled scalar field  $\phi$  with a general kinetic term [90]. For the specific case of a constant sound speed  $c_s^2$ , the Lagrangian density is written as [91]:

$$P(X, \phi) = \left( \frac{X}{A} \right)^{\frac{1-c_s^2}{2c_s^2}} X - V(\phi), \quad (2)$$

where  $X = -\nabla^2\phi/2$  and  $A$  is a constant density scale [40]. In this category of models,  $w_{\text{ADE}} \rightarrow c_s^2$  if the kinetic term dominates, whereas  $w_{\text{ADE}} \rightarrow -1$  if the potential  $V(\phi)$  dominates. The main advantage of the ADE model over the axion-like EDE model is that the former provides a general class of exact solutions, while the latter requires a specific set of initial conditions to achieve a similar phenomenology [40].

Since the ADE equation-of-state parameter changes over time, the conservation equation gives

$$\rho_{\text{ADE}}(a) = \rho_{\text{ADE},0} e^{3 \int_a^1 [1+w_{\text{ADE}}(a')] da'/a'}, \quad (3)$$

which allows us to define the ADE fractional energy density as

$$f_{\text{ADE}}(a) = \frac{\rho_{\text{ADE}}(a)}{\rho_{\text{tot}}(a)}. \quad (4)$$

In Fig. 1, we also plot the evolution of  $f_{\text{ADE}}$  as a function of the cosmological redshift  $z$ . We notice that this parameter is maximal around the ADE equation-of-state transition, set by the critical redshift  $z_c$ , namely, when  $f_{\text{ADE}}(z \sim z_c)$ . Then, this parameter becomes subdominant at the time of recombination, with  $f_{\text{ADE}}(z_*) \sim 1\%$  [92].

Finally, the ADE model we are considering is described by the three following parameters

$$\{z_c, f_{\text{ADE}}(z_c), w_f\}. \quad (5)$$

Ref. [40] also considers the variation of a fourth parameter that determines the behavior of the ADE perturbations, namely, their rest frame sound speed  $c_s^2(k, a)$ . Unlike the standard axion-like EDE model (see below), we assume for this model the scale independence of this parameter, *i.e.*,  $c_s^2(k, a) = c_s^2(a)$ , which is equivalent to assuming a perfect fluid with a linear dispersion relation. In addition, because of the sharp transition of the  $w_{\text{ADE}}$  parameter, the impact of the ADE component on the perturbed universe is localized in time, which implies that we can approximate this parameter as a constant. Thus, Ref. [40] varies this parameter to its critical redshift value, namely,  $c_s^2 = c_s^2(a = a_c)$ , in addition to the three other parameters listed above. In our baseline model, we consider that  $c_s^2 = w_f$ , insofar as it has been shown to

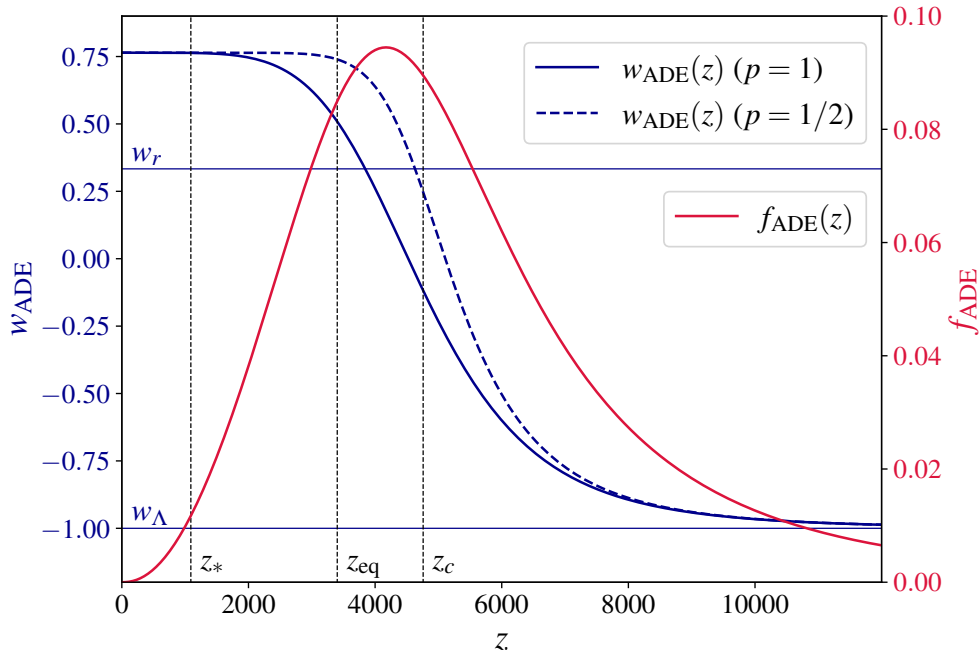


FIG. 1. Evolution of the ADE equation-of-state parameter  $w_{\text{ADE}}$ , as well as the ADE fractional energy density  $f_{\text{ADE}}(z_c)$  as a function of the cosmological redshift  $z$ . To perform this plot, we use the best-fit values of the BAO/ $f\sigma_8$  + Pan +  $M_b$  analysis (see Tab. I). For the ADE equation-of-state parameter, we set  $p = 1$ , which corresponds to our baseline setup, and  $p = 1/2$ , which corresponds to the setup of Ref. [40]. The horizontal lines correspond to the radiation and dark energy equation-of-state parameters,  $w_r$  and  $w_\Lambda$ , respectively, while the dashed vertical lines correspond to the redshift of recombination  $z_*$ , the redshift of the matter-radiation equality  $z_{\text{eq}}$ , and the ADE critical redshift  $z_c$ .

be a good approximation near the best-fit [40]. However, in Sec. IV, we consider two model variations of our baseline model: (i) the  $c_s^2$ ADE model, where we free these two parameters independently, and (ii) the cADE model, where we set  $c_s^2 = w_f = 1$ . Let us note that there exists a second difference between Refs. [40, 41] and our baseline analysis, since these references set  $p = 1/2$ , which leads to a sharper transition than ours (with  $p = 1$ ), as shown in Fig. 1. However, the impact of this parameter on cosmological results is very minor, and we have verified that we obtain the same results as Ref. [41] with  $p = 1$ .

### B. Review of the axion-like EDE model

For comparison, we also consider the axion-like early dark energy (EDE) model [16–18], which corresponds to an extension of the  $\Lambda$ CDM model, where the existence of an additional subdominant oscillating scalar field  $\phi$  is considered. The EDE field dynamics is described by the Klein-Gordon equation of motion (at the homogeneous level),

$$\ddot{\phi} + 3H\dot{\phi} + V_{n,\phi}(\phi) = 0, \quad (6)$$

where  $V_n(\phi)$  is a modified axion-like potential defined as

$$V_n(\phi) = m^2 f^2 [1 - \cos(\phi/f)]^n. \quad (7)$$

$f$  and  $m$  correspond to the decay constant and the effective mass of the scalar field, respectively, while the parameter  $n$  controls the rate of dilution after the field becomes dynamical. In the following, we will use the redefined field quantity  $\Theta = \phi/f$  for convenience, such that  $-\pi \leq \Theta \leq +\pi$ . At early times, when  $H \gg m$ , the scalar field  $\phi$  is frozen at its initial value since the Hubble friction prevails, which implies that the EDE behaves like a form of dark energy and that its contribution to the total energy density increases relative to the other components. When the Hubble parameter drops below a critical value ( $H \sim m$ ), the field starts evolving toward the minimum of the potential and becomes dynamical. The EDE contribution to the total budget of the Universe is maximum around a critical redshift  $z_c$ , after which the energy density starts to dilute with an equation-of-state parameter  $w_{\text{EDE}}(a)$  approximated by [89, 93]:

$$w_{\text{EDE}} = \begin{cases} -1 & \text{if } z > z_c, \\ \frac{n-1}{n+1} & \text{if } z < z_c. \end{cases} \quad (8)$$

In the following, we will fix  $n = 3$  as it was found that the data were relatively insensitive to this parameter provided  $2 \lesssim n \lesssim 5$  [18], implying that in this specific model

$w_{\text{EDE}}(z \ll z_c) = 1/2$ . Instead of the theory parameters  $f$  and  $m$ , we make use of  $z_c$  and  $f_{\text{EDE}}(z_c)$ , determined through a shooting method [18]. We also include the initial field value  $\Theta_i$  as a free parameter, whose main role once  $f_{\text{EDE}}(z_c)$  and  $z_c$  are fixed is to set the dynamics of perturbations right around  $z_c$ , through the EDE sound speed  $c_s^2$ . Finally, the axion-like EDE model is described by the three following parameters:

$$\{z_c, f_{\text{EDE}}(z_c), \Theta_i\}. \quad (9)$$

Let us note that the axion-like EDE sound speed  $c_s^2(a, k) = \delta P_{\text{EDE}}(k, a) / \delta \rho_{\text{EDE}}(k, a)$  is scale and time dependent, and is entirely determined by the three EDE parameters specified above. In the fluid approximation, one can estimate the  $a$  and  $k$  dependencies of this parameter as [17, 89]

$$c_s^2(a, k) = \begin{cases} 1, & a \leq a_c, \\ \frac{2a^2(n-1)\varpi^2(a) + k^2}{2a^2(n+1)\varpi^2(a) + k^2}, & a > a_c, \end{cases} \quad (10)$$

where  $\varpi$  corresponds to the angular frequency of the oscillating background field, which has a time dependency fixed by  $z_c$ ,  $n$  and  $\Theta_i$  (see Ref. [89]). Let us note however that the axion-like EDE model we consider in this paper does not rely on this fluid approximation, and instead solves the exact (linearized) Klein-Gordon equation, which is expressed in synchronous gauge as [94]:

$$\delta\phi_k'' + 2H\delta\phi_k' + [k^2 + a^2 V_{n,\phi\phi}] \delta\phi_k = -h'\phi'/2, \quad (11)$$

where the prime denotes derivatives with respect to conformal time.

### C. Data and analysis methods

We perform Markov chain Monte Carlo (MCMC) analyses, confronting the ADE model with recent cosmological observations. To do so, we make use of the Metropolis-Hastings algorithm from the `MontePython-v3`<sup>2</sup> code [95, 96] interfaced with our modified `CLASS` [97, 98] version.<sup>3</sup> In this paper, we perform various analyses from a combination of the following datasets:

- **Planck:** The low- $\ell$  CMB temperature and polarization autocorrelations (TT, EE), and the high- $\ell$  TT, TE, EE data [99], as well as the gravitational lensing potential reconstruction from *Planck* 2018 [100].

<sup>2</sup> [https://github.com/brinckmann/montepython\\_public](https://github.com/brinckmann/montepython_public).

<sup>3</sup> <https://github.com/PoulinV/AxiCLASS>.

- **ext-BAO:** The low- $z$  BAO data gathered from 6dFGS at  $z = 0.106$  [101], SDSS DR7 at  $z = 0.15$  [102].
- **BOSS BAO/ $f\sigma_8$ :** BAO measurements, cross-correlated with the redshift space distortion measurements from the CMASS and LOWZ galaxy samples of BOSS DR12 LRG at  $z = 0.38, 0.51$ , and  $0.61$  [42].
- **eBOSS BAO/ $f\sigma_8$ :** BAO measurements, cross-correlated with the redshift space distortion measurements from the CMASS and LOWZ quasar samples of eBOSS DR16 QSO at  $z = 1.48$  [43].
- **EFTofBOSS:** The EFTofLSS analysis of BOSS DR12 LRG cross-correlated with the reconstructed BAO parameters [103]. The SDSS-III BOSS DR12 galaxy sample data and covariances are described in [42, 104]. The measurements, obtained in [73], are from BOSS catalogs DR12 (v5) combined CMASS-LOWZ [105], and are divided in redshift bins LOWZ,  $0.2 < z < 0.43$  ( $z_{\text{eff}} = 0.32$ ), and CMASS,  $0.43 < z < 0.7$  ( $z_{\text{eff}} = 0.57$ ), with north and south galactic skies for each, respectively, denoted NGC and SGC. From these data we use the monopole and quadrupole moments of the galaxy power spectrum. The theory prediction and likelihood for the full-modeling information are made available through `PyBird` [68], together with the West-coast parametrization [71, 83, 106] as implemented in Ref. [68]. In our analyses, we vary 7 EFT parameters per sky cut, namely, 3 bias parameters ( $b_1, b_3$ , and  $c_2 \equiv (b_2 + b_4)/\sqrt{2}$ ), 2 counterterm parameters ( $c_{\text{ct}}$  and  $c_{r,1}$ ), and 2 stochastic parameters ( $c_{\epsilon,0}$  and  $c_{\epsilon}^{\text{quad}}$ ). The physical meaning of these parameters and the priors used are described in detail in Ref. [83]. Finally, we analyse the BOSS data up to  $k_{\text{max}}^{\text{CMASS}} = 0.23h \text{ Mpc}^{-1}$  for the CMASS sky cut and up to  $k_{\text{max}}^{\text{LOWZ}} = 0.20h \text{ Mpc}^{-1}$  for the LOWZ sky cut (as determined in Ref. [67]).
- **EFTofeBOSS:** The EFTofLSS analysis [65] of eBOSS DR16 QSOs [43]. The QSO catalogs are described in [107] and the covariances are built from the EZ-mocks described in [108]. There are about 343 708 quasars selected in the redshift range  $0.8 < z < 2.2$ , with  $z_{\text{eff}} = 1.52$ , divided into two skies, NGC and SGC [109, 110]. From these data, we use the monopole and quadrupole moments of the galaxy power spectrum. The theory prediction and likelihood for the full-modeling information are made available through `PyBird`, together with the West-coast parametrization as implemented in Ref. [65]. We use the same EFT parameters as for EFTofBOSS, and we set  $k_{\text{max}}^{\text{eBOSS}} = 0.24h \text{ Mpc}^{-1}$  (as determined in Ref. [65]).
- **Pantheon:** The Pantheon catalog of uncalibrated luminosity distance of type Ia supernovae (SNeIa)

in the range  $0.01 < z < 2.3$  [111].

- **Pantheon+**: The newer Pantheon+ catalog of uncalibrated luminosity distance of SNeIa in the range  $0.001 < z < 2.26$  [44].
- **Pantheon+/ $SH_0ES$** : The Pantheon+ catalog cross-correlated with the absolute calibration of the SNeIa from  $SH_0ES$  [2].
- **$M_b$** : Gaussian prior from the most up-to-date late-time measurement of the absolute calibration of the SNeIa from  $SH_0ES$ ,  $M_b = -19.253 \pm 0.027$  [2], corresponding to  $H_0 = (73.04 \pm 1.04)$  km/s/Mpc.

We choose *Planck* + ext-BAO + BOSS BAO/ $f\sigma_8$  + eBOSS BAO/ $f\sigma_8$  + Pantheon (optionally with the  $M_b$  prior) as our baseline analysis, called, for the sake of simplicity, “BAO/ $f\sigma_8$  + Pan.” In order to assess the impact of the EFT full-shape analysis of the BOSS and eBOSS data on the ADE resolution of the Hubble tension, we compare the baseline analysis with an equivalent analysis that includes the EFTofBOSS and EFTofeBOSS likelihoods instead of the BOSS and eBOSS BAO/ $f\sigma_8$  likelihoods. This analysis is called “EFT + Pan.” Finally, in order to gauge the influence of the new Pantheon data, we replace the Pantheon likelihood with the Pantheon+ likelihood. This analysis, referred to as “EFT + PanPlus,” is compared with the aforementioned EFTofLSS analysis. In App. A, we show explicitly that the addition of the  $M_b$  prior on top of the Pantheon+ likelihood is equivalent to the use of the full “Pantheon+/ $SH_0ES$ ” likelihood as provided in Ref. [2].

For all runs performed, we impose large flat priors on  $\{\omega_b, \omega_{\text{cdm}}, H_0, A_s, n_s, \tau_{\text{reio}}\}$ , which correspond, respectively, to the dimensionless baryon energy density, the dimensionless cold dark matter energy density, the Hubble parameter today, the variance of curvature perturbations centered on the pivot scale  $k_p = 0.05$  Mpc $^{-1}$  (according to the *Planck* convention), the scalar spectral index, and the reionization optical depth. Regarding the free parameters of the ADE model, we impose logarithmic flat priors on  $z_c$ , and flat priors on  $f_{\text{ADE}}(z_c)$  and  $w_{\text{ADE}}$ ,

$$\begin{aligned} 3 &\leq \log_{10}(z_c) \leq 4.5, \\ 0 &\leq f_{\text{ADE}}(z_c) \leq 0.2, \\ 0 &\leq w_f \leq 3.6. \end{aligned}$$

Note that we have verified that a wider prior on  $w_f$  does not impact our results. When we compare the ADE model with the axion-like EDE model, we use the following priors for the latter:

$$\begin{aligned} 3 &\leq \log_{10}(z_c) \leq 4, \\ 0 &\leq f_{\text{EDE}}(z_c) \leq 0.5, \\ 0 &\leq \Theta_i \leq \pi. \end{aligned}$$

In this paper, we use *Planck* conventions for the treatment of neutrinos; that is, we include two massless and

one massive species with  $m_\nu = 0.06$  eV [1]. In addition, we use *Hmcode* [112] to estimate the nonlinear matter clustering solely for the purpose of the CMB lensing. We define our MCMC chains to be converged when the Gelman-Rubin criterion  $R - 1 < 0.05$ . Finally, we extract the best-fit parameters from the procedure highlighted in the appendix of Ref. [15], and we produce our figures thanks to *GetDist* [113].

In this paper, we compare the models with each other using two main metrics. First, in order to assess the ability of an extended model  $\mathcal{M}$  to fit all the cosmological data, we compute the Akaike information criterion (AIC) of this model relative to that of the  $\Lambda$ CDM. This metric is defined as follows

$$\Delta\text{AIC} = \chi_{\text{min}, \mathcal{M}}^2 - \chi_{\text{min}, \Lambda\text{CDM}}^2 + 2 \cdot (N_{\mathcal{M}} - N_{\Lambda\text{CDM}}), \quad (12)$$

where  $\mathcal{M} \in \{\text{ADE}, \text{EDE}, c_s^2\text{ADE}, \text{cADE}\}$ , and where  $N_{\mathcal{M}}$  stands for the number of free parameters of the model. This metric enables us to determine whether the fit within a particular model  $\mathcal{M}$  significantly improves that of  $\Lambda$ CDM by penalizing models with a larger number of degrees of freedom. Second, in order to gauge the ability of the extended model  $\mathcal{M}$  to solve the Hubble tension for a given combination of data  $\mathcal{D}$  (which does not include the  $M_b$  prior), we also compute the residual Hubble tension thanks to the difference of the maximum *a posteriori* (DMAP) [114], determined by

$$Q_{\text{DMAP}} = \sqrt{\chi_{\text{min}, \mathcal{M}}^2(\mathcal{D} + M_b) - \chi_{\text{min}, \mathcal{M}}^2(\mathcal{D})}. \quad (13)$$

This metric allows us to determine how the addition of the  $M_b$  prior to the dataset  $\mathcal{D}$  impacts the fit within a particular model  $\mathcal{M}$ . Ref. [15] asserts that a model is a good candidate for solving the Hubble tension if it meets these two conditions:  $\Delta\text{AIC} < -6.91$  and  $Q_{\text{DMAP}} < 3\sigma$ . Finally, we also consider the Gaussian tension (GT), computed as

$$\text{GT} = \frac{\overline{H_0}(\text{SH}_0\text{ES}) - \overline{H_0}(\mathcal{D})}{\sqrt{\sigma_{H_0}^2(\text{SH}_0\text{ES}) + \sigma_{H_0}^2(\mathcal{D})}}, \quad (14)$$

where  $\overline{H_0}$  and  $\sigma_{H_0}$  correspond to the mean and standard deviation of the Hubble parameter today determined from the  $SH_0ES$  experiment and the dataset  $\mathcal{D}$  (within the model  $\mathcal{M}$ ). The Gaussian tension is certainly the most direct metric for quantifying the Hubble tension, but the main problem with this metric is that it is unable to favor a complex model in which some parameters become irrelevant in the  $\Lambda$ CDM limit. If a probability density function deviates from Gaussian in a complex model (as is the case for EDE models), only the Gaussian  $\Lambda$ CDM limit has significant statistical weight [15, 86].

### III. COSMOLOGICAL RESULTS

In this section, we discuss the cosmological constraints of the ADE and axion-like EDE models and their ability

	BAO/ $f\sigma_8$ + Pan		EFT + Pan		EFT + PanPlus	
	No	Yes	No	Yes	No	Yes
$M_b$ prior?						
$f_{\text{ADE}}(z_c)$	< 0.060(0.034)	0.081(0.090) $\pm$ 0.018	< 0.049(0.010)	0.068(0.076) $\pm$ 0.019	< 0.036(0.011)	0.073(0.082) $\pm$ 0.020
$\log_{10}(z_c)$	unconst.(3.748)	3.655(3.677) $\pm$ 0.093	unconst.(3.713)	3.676(3.686) $^{+0.095}_{-0.120}$	unconst.(3.957)	3.692(3.724) $^{+0.098}_{-0.120}$
$w_f$	> 0.49(0.69)	0.79(0.76) $^{+0.10}_{-0.12}$	> 0.59(0.70)	0.78(0.75) $^{+0.11}_{-0.13}$	> 0.61(0.57)	0.76(0.73) $\pm$ 0.13
$H_0$	68.44(69.04) $^{+0.47}_{-0.93}$	71.24(71.49) $\pm$ 0.68	68.16(68.26) $^{+0.41}_{-0.53}$	71.01(71.31) $\pm$ 0.73	68.03(68.16) $^{+0.43}_{-0.53}$	71.13(71.29) $\pm$ 0.73
$\omega_{\text{cdm}}$	0.1212(0.1239) $^{+0.0012}_{-0.0030}$	0.1291(0.1305) $\pm$ 0.0027	0.1196(0.1202) $^{+0.0009}_{-0.0015}$	0.1267(0.1280) $\pm$ 0.0027	0.1201(0.1211) $^{+0.0011}_{-0.0015}$	0.1278(0.1294) $\pm$ 0.0028
$10^2\omega_b$	2.259(2.269) $^{+0.016}_{-0.023}$	2.304(2.309) $\pm$ 0.021	2.254(2.252) $^{+0.014}_{-0.017}$	2.303(2.306) $\pm$ 0.022	2.250(2.258) $\pm$ 0.018	2.306(2.311) $\pm$ 0.022
$10^9 A_s$	2.123(2.119) $\pm$ 0.030	2.159(2.152) $\pm$ 0.031	2.111(2.111) $\pm$ 0.030	2.148(2.151) $^{+0.028}_{-0.032}$	2.111(2.116) $^{+0.028}_{-0.036}$	2.151(2.150) $^{+0.028}_{-0.033}$
$n_s$	0.9711(0.9748) $^{+0.0041}_{-0.0074}$	0.9900(0.9925) $\pm$ 0.0061	0.9684(0.9686) $^{+0.0040}_{-0.0048}$	0.9878(0.9904) $\pm$ 0.0060	0.9679(0.9697) $^{+0.0038}_{-0.0047}$	0.9890(0.9906) $\pm$ 0.0063
$\tau_{\text{reio}}$	0.0583(0.0540) $^{+0.0063}_{-0.0075}$	0.0588(0.0561) $^{+0.0066}_{-0.0077}$	0.0572(0.0573) $\pm$ 0.0070	0.0590(0.0584) $^{+0.0067}_{-0.0077}$	0.0570(0.0574) $\pm$ 0.0072	0.0585(0.0573) $^{+0.0065}_{-0.0077}$
$S_8$	0.828(0.834) $^{+0.011}_{-0.013}$	0.843(0.846) $\pm$ 0.013	0.820(0.823) $\pm$ 0.010	0.832(0.835) $\pm$ 0.012	0.825(0.830) $^{+0.010}_{-0.011}$	0.836(0.842) $\pm$ 0.013
$\Omega_m$	0.3083(0.3089) $\pm$ 0.0054	0.3011(0.3018) $\pm$ 0.0050	0.3074(0.3078) $\pm$ 0.0050	0.2983(0.2983) $\pm$ 0.0047	0.3096(0.3107) $^{+0.0047}_{-0.0053}$	0.2994(0.3014) $\pm$ 0.0047
$\Delta\chi^2_{\text{min}}$	-3.9	-28.3	-1.4	-24.9	-1.3	-27.8
$\Delta\text{AIC}$	+2.1	-22.3	+4.6	-18.9	+4.7	-21.8
$Q_{\text{DMAP}}$		2.6 $\sigma$		2.9 $\sigma$		3.6 $\sigma$
$Q_{\text{DMAP}}(\text{EDE})$		1.5 $\sigma$		2.4 $\sigma$		2.5 $\sigma$
$Q_{\text{DMAP}}(\Lambda\text{CDM})$		5.6 $\sigma$		5.6 $\sigma$		6.3 $\sigma$

TABLE I. Mean (best-fit)  $\pm 1\sigma$  (or  $2\sigma$  for one-sided bounds) of reconstructed parameters in the ADE model confronted to various datasets. All datasets include *Planck* + ext-BAO data, while we consider either the BAO/ $f\sigma_8$  information or the EFT full-shape analysis for the BOSS and eBOSS data, and we consider either the Pantheon data or the Pantheon+ data (with and without the  $M_b$  prior). We also display for all datasets the  $\Delta\chi^2_{\text{min}}$  with respect to  $\Lambda\text{CDM}$ , the associated  $\Delta\text{AIC}$ , as well as the  $Q_{\text{DMAP}}$ . Finally,  $Q_{\text{DMAP}}(\Lambda\text{CDM})$  and  $Q_{\text{DMAP}}(\text{EDE})$  corresponds to the  $Q_{\text{DMAP}}$  of the  $\Lambda\text{CDM}$  and axion-like EDE models for the equivalent datasets.

to solve the Hubble tension by successively evaluating the impact of the EFT full-shape analysis of the BOSS and eBOSS data (compared with the standard BAO/ $f\sigma_8$  analysis) and the impact of the new Pantheon data (compared with the equivalent older data) on these models. The cosmological constraints for the ADE model are shown in Tab. I, while the  $\chi^2_{\text{min}}$  values associated with each likelihood are presented in Tab. III of App. B. In Tab. I, we also display the  $\Delta\chi^2_{\text{min}}$  and the associated  $\Delta\text{AIC}$  with respect to  $\Lambda\text{CDM}$ , as well as the  $Q_{\text{DMAP}}$  for several combinations of data.

Our baseline combination of data, denoted “BAO/ $f\sigma_8$  + Pan,” refers to *Planck* + ext-BAO + BOSS BAO/ $f\sigma_8$  + eBOSS BAO/ $f\sigma_8$  + Pantheon, corresponding roughly to that used in Ref. [41].<sup>4</sup> For this analysis, combined with the  $M_b$  prior, we find  $f_{\text{ADE}}(z_c) = 0.081 \pm 0.018$  and  $H_0 = 71.24 \pm 0.68$  km/s/Mpc for the ADE model, leading to a residual Hubble tension of  $Q_{\text{DMAP}} = 2.6\sigma$  and a preference over  $\Lambda\text{CDM}$  of  $\Delta\text{AIC} = -22.3$  (see Tab. I). Note that this  $\chi^2$  improvement is mainly driven by the  $SH_0\text{ES}$  data (as is also the case in the remainder of this paper), implying that this preference over  $\Lambda\text{CDM}$  will no longer be significant if the Hubble tension is due to a systematic error in the data. Let us underline that with our baseline combination of data, the ADE model satisfies both Ref. [15] conditions. In addition, we find for the ADE model that  $\text{GT} = 3.7\sigma$  for our original combination of data. We are now assessing how the EFTofLSS on the one hand, and the new data from Pantheon+ on the other hand, change these conclusions.

### A. Impact of the EFTofLSS analysis

In the top panel of Fig. 2, we show the reconstructed 2D posteriors of the ADE model for the analysis with the BOSS and eBOSS BAO/ $f\sigma_8$  likelihoods (namely, the BAO/ $f\sigma_8$  + Pan analysis), as well as for the analysis with the EFTofBOSS and EFTofeBOSS likelihoods (namely, the EFT + Pan analysis), either with or without the  $M_b$  prior. To isolate the effect of the EFT full-shape analysis, we carry out these analyses using only the older Pantheon data.

For the analyses without the  $M_b$  prior, the addition of the EFT likelihood has a non-negligible impact on the  $f_{\text{ADE}}(z_c)$ ,  $w_f$ , and  $H_0$  constraints. The upper bound of the ADE fractional energy density and the lower bound of  $w_f$  are indeed both improved by  $\sim 20\%$ , while the standard deviation of  $H_0$  is reduced by  $\sim 35\%$ .

When we consider the  $M_b$  prior, EFTofBOSS and EFTofeBOSS do not improve the parameter constraints of this model over the BAO/ $f\sigma_8$  information. However, these likelihoods shift  $f_{\text{ADE}}(z_c)$  and  $H_0$  toward smaller values of  $0.7\sigma$  and  $0.3\sigma$ ,<sup>5</sup> respectively. The EFT full-shape analysis of the BOSS and eBOSS data therefore slightly reduces the ability of this model to resolve the Hubble tension, and the  $Q_{\text{DMAP}}$  changes from  $2.6\sigma$  to  $2.9\sigma$  when EFT likelihoods are considered (see Tab. I). In particular, the  $\chi^2_{\text{min}}$  associated with the  $M_b$  prior is

<sup>4</sup> Note that this analysis used another  $SH_0\text{ES}$  prior,  $H_0 = 74.03 \pm 1.42$  km/s/Mpc, from Ref. [115], and does not take into account the redshift space distortion information (but only the BAO).

<sup>5</sup> Since we are considering here the same experiments (with different methods for extracting cosmological constraints), we use the following metric:  $2 \cdot (\theta_i - \theta_j) / (\sigma_{\theta,i} + \sigma_{\theta,j})$ , where  $\theta_i$  and  $\sigma_{\theta,i}$  are, respectively, the mean value and the standard deviation of the parameter  $\theta$  for the dataset  $i$ .

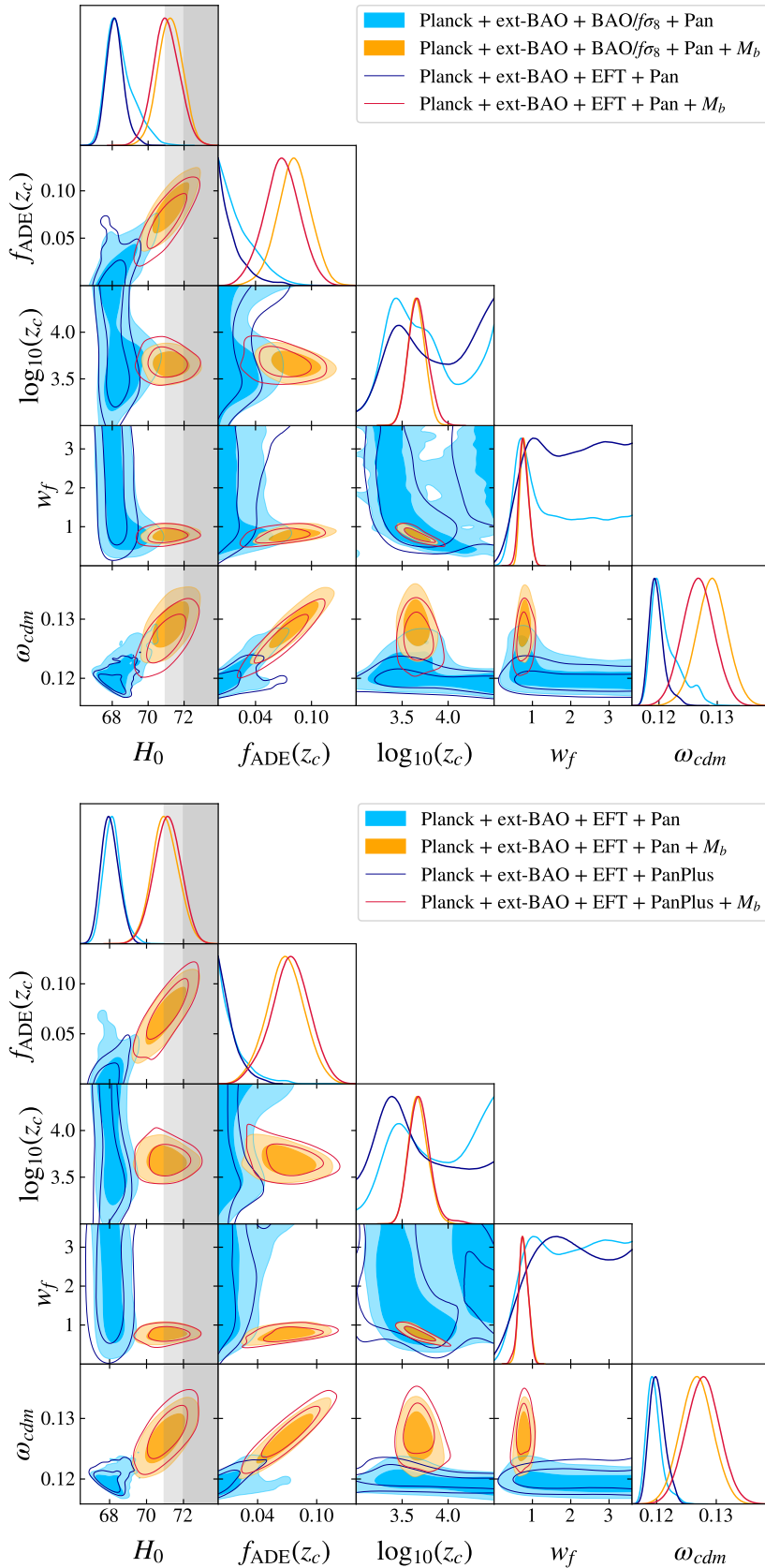


FIG. 2. *Top panel:* 2D posterior distributions reconstructed from the BAO/ $f\sigma_8$  + Pan dataset compared with the 2D posterior distributions reconstructed from the EFT + Pan dataset, either with or without the  $M_b$  prior. *Bottom panel:* 2D posterior distributions reconstructed from the EFT + Pan dataset compared with the 2D posterior distributions reconstructed from the EFT + PanPlus dataset, either with or without the  $M_b$  prior. The gray bands correspond to the  $H_0$  constraint associated with the  $M_b$  prior, namely,  $H_0 = (73.04 \pm 1.04)$  km/s/Mpc [2].

degraded by 1.0 compared to the BAO/ $f\sigma_8$  analysis. In addition, the preference for this model over the  $\Lambda$ CDM model is slightly reduced, given that the  $\Delta$ AIC changes from  $-22.3$  to  $-18.9$  when the EFT likelihood is added (see Tab. I). Note that at this point, the ADE model still satisfies both conditions of Ref. [15], even though  $Q_{\text{DMAP}} \sim 3\sigma$ . However, the Gaussian tension changes from  $3.7\sigma$  to  $4.3\sigma$  when EFT likelihoods are considered, which can be explained by the fact that the  $f_{\text{ADE}}(z_c)$  parameter is better constrained by the EFT + Pan dataset.

For the axion-like EDE case, we find for the equivalent analyses (see Tab. III of App. B) that the  $Q_{\text{DMAP}}$  changes from  $1.5\sigma$  to  $2.4\sigma$ , and that the  $\Delta$ AIC changes from  $-29.1$  to  $-22.9$ , when EFT likelihoods are added.<sup>6</sup> The ADE model slightly better supports the addition of the EFT likelihood compared to the EDE model, insofar as the  $Q_{\text{DMAP}}$  and  $\Delta$ AIC are more stable (see Tab. I). However, the EDE model remains a better model to solve the Hubble tension, with  $Q_{\text{DMAP}} = 2.4\sigma$  for the EFT + Pan analysis, compared to  $Q_{\text{DMAP}} = 2.9\sigma$  for the ADE model, and has a better fit to the data when the  $M_b$  prior is added, with  $\Delta$ AIC =  $-22.9$ , compared to  $\Delta$ AIC =  $-18.9$  for the ADE model. For a detailed discussion of the EFTofLSS impact on the EDE model in the framework of the BOSS data, please refer to Ref. [84].<sup>7</sup>

## B. Impact of the Pantheon+ data

Let us now turn to the impact of the latest Pantheon data, namely, the Pantheon+ data, on the ability of these models to resolve the Hubble tension. In the bottom panel of Fig. 2, we show the reconstructed 2D posteriors of the ADE model for the analyses with the old Pantheon data (*i.e.*, the EFT + Pan analysis), as well as for the analyses with the updated data (*i.e.*, the EFT + PanPlus analysis). To isolate the effect of the Pantheon+ data, we carry out these analyses using only the EFT full-shape analysis of the BOSS and eBOSS data.

The analysis with the Pantheon+ data, but without any  $SH_0$ ES prior, improves significantly the 95% C.L.

constraints on  $f_{\text{ADE}}(z_c)$  by  $\sim 30\%$ . This implies that  $H_0$  is shifted down by  $0.2\sigma$ <sup>8</sup> compared to the analysis with the old Pantheon data. Although the ADE model prefers a higher value of  $\omega_{\text{cdm}}$  than  $\Lambda$ CDM (because ADE slows down the evolution of the growing modes), the larger  $\Omega_m$  favored by the Pantheon+ data ( $\Omega_m = 0.334 \pm 0.018$  [44]) leads to a large  $\omega_{\text{cdm}} = \Omega_{\text{cdm}} \cdot h^2$  which is not sufficiently compensated for by ADE. Then, to offset the high value of  $\Omega_m$ , the current Hubble parameter decreases slightly, as well as  $f_{\text{ADE}}(z_c)$ , since the latter is positively correlated with  $H_0$ .

When the  $M_b$  prior is included, nonzero contributions of ADE are favored. One may have expected that the tighter constraints from Pantheon+ may reduce the contribution of  $f_{\text{ADE}}$  and the value of  $H_0$ . These are in fact stable when compared to analyses with the older Pantheon data, with similar error bars between the EFT + Pan +  $M_b$  and EFT + PanPlus +  $M_b$  analyses. Thus, if we rely solely on the posterior distributions, we could argue that the Pantheon+ data do not change the conclusion about the ADE resolution of the Hubble tension. However, it turns out that the ADE model is not able to accommodate at the same time the large values of  $H_0$  and  $\Omega_m$  that are favored by the Pantheon+ data once they are calibrated with  $M_b$ . Indeed, the best-fit value  $H_0 = 71.29$  km/s/Mpc is  $1.7\sigma$  lower than the  $SH_0$ ES constraint [ $H_0 = (73.04 \pm 1.04)$  km/s/Mpc], while the best-fit value  $\Omega_m = 0.3014$  is  $1.8\sigma$  lower than the Pantheon+ constraint ( $\Omega_m = 0.334 \pm 0.018$ ). Therefore, the ADE model does not provide a good fit to the  $M_b$  prior ( $\chi^2_{M_b} = 6.42$  as shown in Tab. III of App. B), while the fit to the Pantheon+ data is worse (by  $+1.6$ ) with the inclusion of the  $M_b$  prior. These degradations of  $\chi^2_{\text{min}}$ <sup>9</sup> imply that the  $Q_{\text{DMAP}}$  changes from  $2.9\sigma$  ( $5.6\sigma$  for  $\Lambda$ CDM) to  $3.6\sigma$  ( $6.3\sigma$  for  $\Lambda$ CDM) when we consider the Pantheon+ data (see Tab. I), which severely limits the ability of this model to resolve the  $H_0$  tension. One of the two criteria of Ref. [15], namely,  $Q_{\text{DMAP}} < 3\sigma$ , is indeed no longer fulfilled. However, while the Pantheon+ data and the  $M_b$  prior from Ref. [2] seriously restrict the ability of the ADE model to resolve the Hubble tension, these data improve the preference for this model over  $\Lambda$ CDM, since the  $\Delta$ AIC changes from  $-18.9$  to  $-21.8$ . We nevertheless caution overinterpreting this preference, given that the  $Q_{\text{DMAP}}$  indicates that combining these datasets is not statistically consistent. In addition, the Gaussian tension  $\text{GT} = 4.4\sigma$  is stable with respect to the EFT +

<sup>6</sup> The similar analysis in Ref. [84], which does not include the eBOSS data, determined that  $Q_{\text{DMAP}} = 2.0\sigma$  for the BAO/ $f\sigma_8$  + Pan analysis and that  $Q_{\text{DMAP}} = 2.1\sigma$  for the EFT + Pan analysis (see Tab. 8 in Ref. [84]). This difference is due solely to the eBOSS data: the  $\chi^2$  of the eBOSS BAO/ $f\sigma_8$  likelihood is improved when the  $M_b$  prior is added (which decreases the  $Q_{\text{DMAP}}$  of the BAO/ $f\sigma_8$  + Pan analysis), while the  $\chi^2$  is degraded for the EFTofBOSS likelihood when the  $M_b$  prior is added (which increases the  $Q_{\text{DMAP}}$  of the EFT + Pan analysis).

<sup>7</sup> Note that Ref [84] used an  $H_0$  prior equivalent to the  $M_b$  prior, and did not consider the EFTofeBOSS likelihood (as well as the eBOSS BAO/ $f\sigma_8$  likelihood). We leave a detailed evaluation of the impact of eBOSS data on the EDE model for future work.

<sup>8</sup> Since we are considering here different experiments, we use the following metric:  $(\theta_i - \theta_j) / \sqrt{\sigma_{\theta,i}^2 + \sigma_{\theta,j}^2}$ , where  $\theta_i$  and  $\sigma_{\theta,i}$  are, respectively, the mean value and the standard deviation of the parameter  $\theta$  for the dataset  $i$ .

<sup>9</sup> Let us note that the  $\chi^2_{\text{min}}$  of the other likelihoods are stable between the Pantheon and Pantheon+ analyses, and therefore play no role in the change in  $Q_{\text{DMAP}}$  between these two analyses.



Pan dataset.<sup>10</sup>

In the left panel of Fig. 4, we show the 2D posterior distributions of the axion-like EDE model reconstructed from the EFT + PanPlus +  $M_b$  dataset, while the associated cosmological constraints are displayed in Tab. II. For the axion-like EDE case, we find that the  $Q_{\text{DMAP}}$  changes from  $2.4\sigma$  to  $2.5\sigma$ , and that the  $\Delta\text{AIC}$  changes from  $-22.9$  to  $-29.1$ , between the old and the new Pantheon data analysis (see Tab. III of App. B for the individual  $\chi^2_{\text{min}}$ ). This model better supports these new data, since the  $Q_{\text{DMAP}}$  is stable (and especially the  $\chi^2_{\text{min}}$  of the  $SH_0\text{ES}$  prior), while the  $\Delta\text{AIC}$ , as in the case of the ADE model, decreases significantly. Whereas with the addition of the EFT data we had a slight preference for EDE over ADE, with the Pantheon+ data the preference for this model becomes clearly apparent: in the axion-like EDE model,  $H_0 = 71.67 \pm 0.77$  km/s/Mpc with  $Q_{\text{DMAP}} = 2.5\sigma$ , while in the ADE model,  $H_0 = 71.13 \pm 0.73$  km/s/Mpc with  $Q_{\text{DMAP}} = 3.6\sigma$ . In addition, the axion-like EDE model provides a better overall fit than the ADE model, with  $\Delta\text{AIC}(\text{EDE} - \text{ADE}) = +7.3$ . The two main contributions to this difference come from the *Planck* data (and in particular the high- $\ell$  TTTEEE likelihood), where  $\Delta\chi^2(\text{EDE} - \text{ADE}) = +3.7$ , and from the  $SH_0\text{ES}$  prior, where  $\Delta\chi^2(\text{EDE} - \text{ADE}) = +2.7$ . The axion-like EDE model is capable of better compensating the effect of large values of  $H_0$  and  $\Omega_m$  (and therefore  $\omega_{\text{cdm}}$ ) on the CMB compared to the ADE model.

In order to understand why the axion-like EDE model performs better than ADE, we plot in Fig. 3 the CMB power spectra residuals with respect to the  $\Lambda\text{CDM}$  best-fit for these two models. In this figure, we also plot (in green dashed) the CMB power spectra residuals of the ADE model, where we set the  $\Lambda\text{CDM}$  parameters to the axion-like EDE best-fit, and the  $z_c$  and  $w_f$  parameters to the ADE best-fit. The last ADE parameter, namely,  $f_{\text{ADE}}(z_c)$ , is determined such that the values of the angular acoustic scale at recombination  $\theta_*$  and the comoving sound horizon at recombination  $r_*$  are the same as for the EDE best-fit. In other words, this plot would represent the best-fit of the ADE model if the latter could reduce the Hubble tension to the same level as the axion-like EDE model. In this figure, the main difference between the ADE and ADE  $\rightarrow$  EDE plots stems from the suppression (particularly at low  $\ell$ ) of the  $C_\ell^{\text{TT}}$  power spectrum for the EDE  $\rightarrow$  ADE analysis. This suppression typically corresponds to the effect of a large value of  $\omega_{\text{cdm}}$  (and also  $n_s$ ), showing that the ADE model is not able to compensate for a high value of  $\Omega_{\text{cdm}}h^2$  in the same way as the axion-like EDE model. This is explained by the fact that the EDE model allows the sound speed to decrease in the

$k$  range associated with  $\ell < 500$ , making it easier to compensate for the effect of increasing  $\Omega_{\text{cdm}}h^2$  in the low- $\ell$  TT power spectrum. Let us note that the effect of the increase in  $\Omega_{\text{cdm}}h^2$  is more significant for the modes that have reentered the horizon at the time when  $f_{\text{ADE}}$  is decreasing, and therefore no longer significantly suppresses the evolution of the growing modes. In order to compensate for this effect, it is therefore helpful to decrease  $c_s^2$  for  $l < 500$ , insofar as a reduction in this parameter leads to an enhancement in the Weyl potential (see Ref. [40]). Note that these results are compatible with Ref. [40], but interestingly the limitation in the value of  $\Omega_{\text{cdm}}h^2$  does not arise from the CMB polarization as in that reference (which considered *Planck* 2015 data), but from the CMB temperature.

## IV. MODEL VARIATIONS

### A. Variation of $c_s^2$

In the previous sections, we fixed  $c_s^2(a_c) = w_f$  instead of varying these two parameters independently. In the right panel of Fig. 4, we show the 2D posterior distributions reconstructed from the EFT + PanPlus +  $M_b$  dataset for our baseline ADE model by relaxing this assumption, while in Tab. II we display the associated cosmological constraints. To do so, we have applied the prior of Refs. [40, 41] to  $c_s^2$ , namely,

$$0 \leq c_s^2 \leq 1.5.$$

In the following, we simply call this extended model “ $c_s^2\text{ADE}$ ,” for which we still consider that  $p = 1$ . Interestingly, and in line with Ref. [40], the assumption  $c_s^2 = w_f$  does not change our conclusions, especially regarding the Hubble tension: we obtain  $Q_{\text{DMAP}} = 3.6\sigma$ , which is similar to that of our baseline ADE model (see Tab. III of App. B for the  $\chi^2$  values). In this specific case, we obtain  $H_0 = 70.76 \pm 0.70$  km/s/Mpc, which is  $0.5\sigma$  lower than the  $H_0$  value from our baseline ADE model. This is due to projection effects caused by the non-Gaussian posteriors of  $c_s^2$  and  $w_f$ , and we notice that the best-fit value ( $H_0 = 71.23$  km/s/Mpc) is very close to that of the ADE model. Thus, the relaxation of this hypothesis does not resolve the Hubble tension, while the  $\Delta\text{AIC}$  worsens somewhat in this model because of the additional parameter ( $\Delta\text{AIC} = -20.1$  instead of  $-21.8$  for our baseline ADE model). In addition, as shown in Fig. 5, the best-fit point of the ADE model in the  $c_s^2 - w_f$  plane lies in the 68% C.L. reconstructed from the  $c_s^2\text{ADE}$  model, and is very close to the best-fit point of this model. This implies that setting  $c_s^2 = w_f$  is a good approximation around the best-fit of the  $c_s^2\text{ADE}$  model.

<sup>10</sup> Note that for the same dataset, we obtain  $\text{GT} = 3.8\sigma$  for the axion-like EDE model and  $\text{GT} = 4.8\sigma$  for the  $\Lambda\text{CDM}$  model.

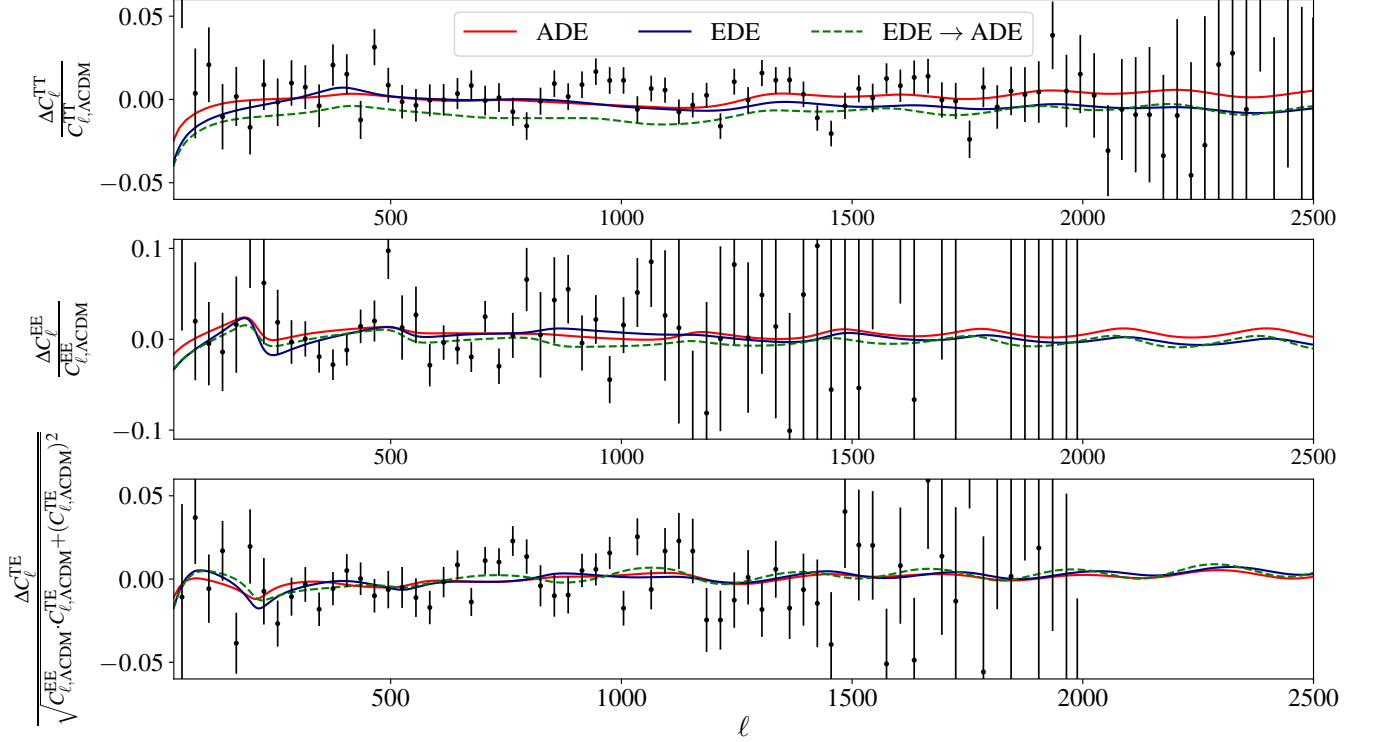


FIG. 3. CMB power spectra residuals with respect to  $\Lambda$ CDM for the ADE (red) and axion-like EDE (black) models. All cosmological parameters of the  $\Lambda$ CDM, ADE, and axion-like EDE models have been set to their EFT + PanPlus best-fits, while the displayed data (normalized to the  $\Lambda$ CDM best-fit) correspond to the *Planck* 2018 data [99]. Finally, for the plot titled “EDE  $\rightarrow$  ADE,” we set the  $\Lambda$ CDM parameters to the axion-like EDE best-fit, while the  $z_c$  and  $w_f$  parameters are set to the ADE best-fit. The last ADE parameter, namely,  $f_{\text{ADE}}(z_c) = 0.095$ , is determined such that the values of  $100\theta_s = 1.042$  and  $r_s = 140.53$  Mpc are the same as for the EDE best-fit.

	EDE	$c_s^2$ ADE	cADE
$f_{\text{ADE/EDE}}(z_c)$	0.116(0.128) $^{+0.023}_{-0.021}$	0.103(0.080) $^{+0.028}_{-0.046}$	0.079(0.087) $\pm$ 0.019
$\log_{10}(z_c)$	3.69(3.84) $^{+0.20}_{-0.16}$	3.61(3.73) $^{+0.12}_{-0.10}$	3.540(3.532) $\pm$ 0.058
$\Theta_i$	2.77(2.88) $^{+0.15}_{-0.072}$	–	–
$w_f$	–	unconst.(0.71)	–
$c_s^2$	–	> 0.701(0.72)	–
$H_0$	71.67(71.84) $\pm$ 0.77	70.76(71.23) $\pm$ 0.70	70.95(71.23) $\pm$ 0.73
$\omega_{\text{cdm}}$	0.1303(0.1309) $\pm$ 0.0030	0.1257(0.1294) $\pm$ 0.0024	0.1273(0.1286) $\pm$ 0.0028
$10^2\omega_b$	2.294(2.312) $\pm$ 0.024	2.304(2.310) $\pm$ 0.020	2.305(2.308) $\pm$ 0.021
$10^9 A_s$	2.149(2.143) $^{+0.027}_{-0.034}$	2.152(2.150) $^{+0.030}_{-0.036}$	2.149(2.158) $\pm$ 0.031
$n_s$	0.9898(0.9951) $\pm$ 0.0061	0.9882(0.9902) $\pm$ 0.0065	0.9849(0.9874) $\pm$ 0.0057
$\tau_{\text{reio}}$	0.0590(0.0590) $^{+0.0063}_{-0.0079}$	0.0592(0.0573) $^{+0.0069}_{-0.0080}$	0.0573(0.0583) $^{+0.0066}_{-0.0078}$
$S_8$	0.836(0.836) $\pm$ 0.011	0.831(0.842) $\pm$ 0.012	0.836(0.841) $\pm$ 0.012
$\Omega_m$	0.2995(0.2997) $\pm$ 0.0047	0.2985(0.3018) $\pm$ 0.0049	0.3000(0.3001) $\pm$ 0.0047
$\Delta\chi_{\text{min}}^2$	–35.1	–27.9	–24.1
$\Delta\text{AIC}$	–29.1	–19.9	–20.1
$Q_{\text{DMAP}}$	2.5 $\sigma$	3.6 $\sigma$	3.9 $\sigma$

TABLE II. Mean (best-fit)  $\pm 1\sigma$  (or  $2\sigma$  for one-sided bounds) of reconstructed parameters in the EDE,  $c_s^2$ ADE, and cADE models confronted to the *Planck* + ext-BAO + EFT + PanPlus +  $M_b$  dataset, *i.e.*, the most up-to-date dataset. We also display for each model the  $\Delta\chi_{\text{min}}^2$  with respect to  $\Lambda$ CDM, the associated  $\Delta\text{AIC}$ , as well as the  $Q_{\text{DMAP}}$ .

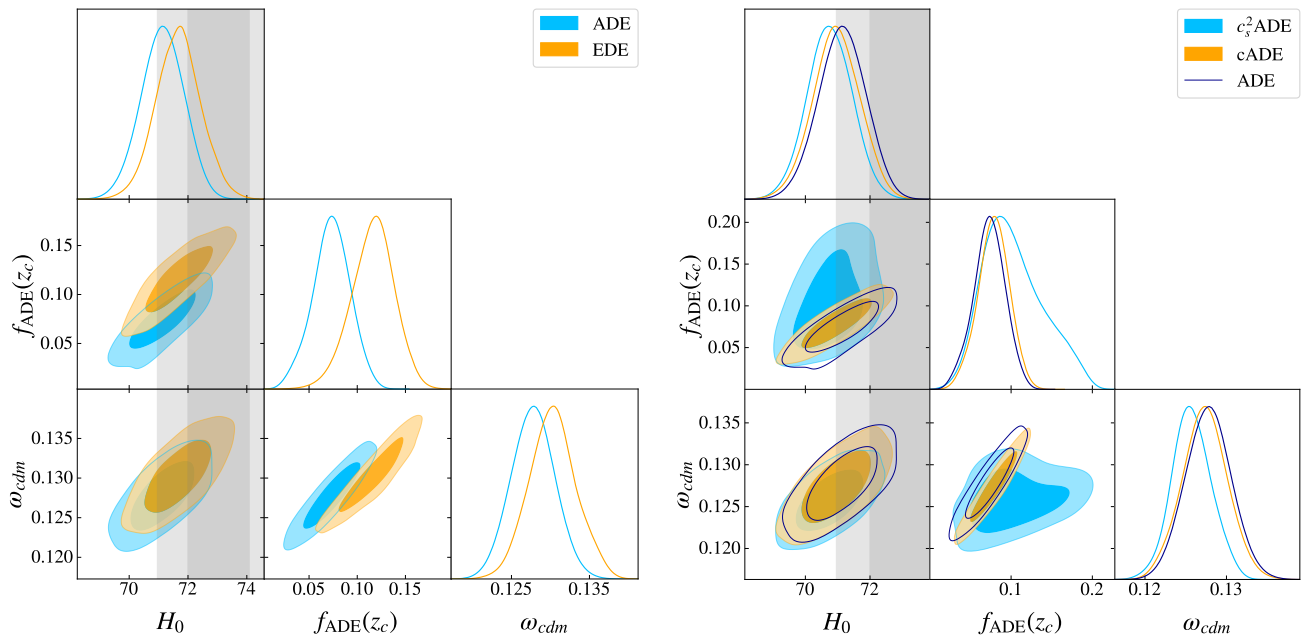


FIG. 4. *Left panel*: 2D posterior distributions reconstructed from the *Planck* + ext-BAO + EFT + PanPlus +  $M_b$  dataset, *i.e.*, the most up-to-date dataset, for our baseline ADE model and the standard axion-like EDE model. *Right panel*: 2D posterior distributions reconstructed from the *Planck* + ext-BAO + EFT + PanPlus +  $M_b$  dataset for the  $c_s^2$ ADE model (namely, our baseline ADE model with the variation of  $c_s^2$ ), the cADE model (namely, our baseline ADE model with  $c_s^2 = w_f = 1$ ), and our baseline ADE model. The gray bands correspond to the  $H_0$  constraint associated with the  $M_b$  prior, namely,  $H_0 = (73.04 \pm 1.04)$  km/s/Mpc [2].

## B. The cADE model

Refs. [40] and [41] showed that the special case where  $c_s^2 = w_f = 1$  made it possible to solve the Hubble tension. In this particular model, called “cADE,” the ADE component is a canonical scalar which goes from a frozen phase ( $w = -1$ ) to a kination phase ( $w = 1$ ) around matter-radiation equality. This model is particularly interesting because it allows the Hubble tension to be resolved with only two more parameters than the  $\Lambda$ CDM model [namely,  $f_{\text{ADE}}(z_c)$  and  $\log_{10}(z_c)$ ]. However, while in Ref. [40] the case  $c_s^2 = w_f = 1$  is within the 68% C.L. of the  $c_s^2$  and  $w_f$  parameters (see Fig. 1 of this reference), one can see in Fig. 5 that this particular case is no longer located in the  $1\sigma$  region.<sup>11</sup> In the right panel of Fig. 4, we display the 2D posterior distributions of the cADE model reconstructed from the EFT + PanPlus +  $M_b$  dataset, while in Tab. II we display the associated cosmological constraints. We can clearly see that this particular model is unable to resolve the Hubble tension with current data, since we obtain  $H_0 = 70.95 \pm 0.73$  km/s/Mpc and  $f_{\text{ADE}}(z_c) = 0.079 \pm 0.019$ , with a  $Q_{\text{DMAP}} = 3.9\sigma$  (compared to  $Q_{\text{DMAP}} = 3.6\sigma$  for our baseline ADE model).

## V. CONCLUSION

In this paper, we have updated the constraints on the acoustic dark energy and axion-like early dark energy models by first assessing the impact of the EFT full-shape analysis applied to the BOSS LRG and eBOSS QSO data, and second the impact of the latest Pantheon+ data.

- When we consider the full-shape analysis of the BOSS and eBOSS data, combined with *Planck*, ext-BAO measurements, Pantheon data from [111], and  $SH_0ES$  data from [2], we obtain  $H_0 = 71.01 \pm 0.73$  km/s/Mpc with a residual Hubble tension of  $2.9\sigma$  (compared to  $2.4\sigma$  for the axion-like EDE model and  $5.6\sigma$  for the  $\Lambda$ CDM model).
- We have demonstrated that the EFTofLSS analysis slightly reduces the ability of this model to resolve the Hubble tension compared to the BAO/ $f\sigma_8$  analysis, which has a residual tension of  $2.6\sigma$  (with  $H_0 = 71.24 \pm 0.68$  km/s/Mpc).
- Although the axion-like EDE model remains a better solution to the Hubble tension after using the EFTofBOSS and EFTofEBOSS likelihoods, we have shown that the EFTofLSS analysis has a stronger impact on this model.
- Importantly, when we replace the Pantheon data with the Pantheon+ data from [44], the ADE

<sup>11</sup> Let us note that Refs. [40, 41] set  $p = 1/2$ , while we set  $p = 1$ , but this difference does not change the results.

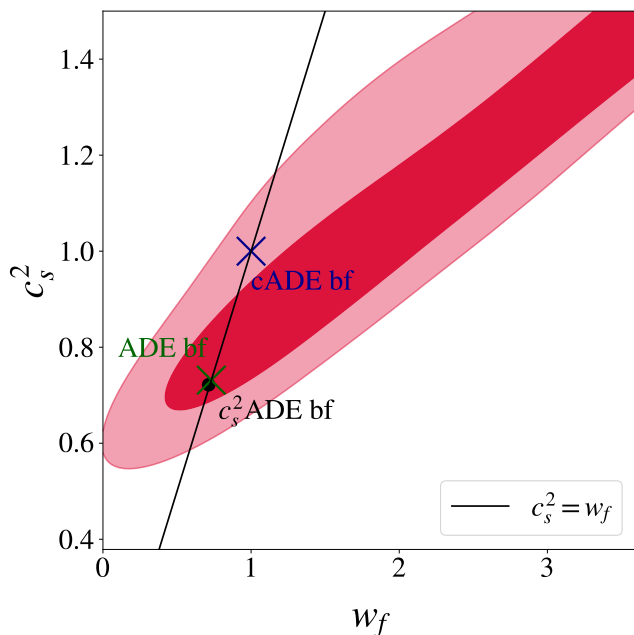


FIG. 5. 2D posterior distribution of the  $c_s^2 - w_f$  plane reconstructed from the *Planck* + ext-BAO + EFT + PanPlus +  $M_b$  dataset for the  $c_s^2$ ADE model. The solid line corresponds to  $c_s^2 = w_f$ , while the blue and green crosses correspond, respectively, to the cADE model and the best-fit of our baseline ADE model. The black circle represents the best-fit of the  $c_s^2$ ADE model.

model no longer resolves the Hubble tension at a suitable level, leading to a  $3.6\sigma$  residual tension (compared to  $2.5\sigma$  for the EDE model and  $6.3\sigma$  for the  $\Lambda$ CDM model).

- Whereas with the EFTofLSS analysis we had only a slight preference for EDE over ADE, with the new data from Pantheon+ and  $SH_0ES$ , the preference for this model became clearly apparent, due to the fact that axion-like EDE manages to compensate a higher  $\Omega_{\text{cdm}}h^2$  in *Planck* data thanks to the scale dependence of the sound speed.
- Finally, we have verified that relaxing the assumption  $c_s^2 = w_f$  does not alter our conclusions, justifying this choice. In addition, for the cADE model (where  $c_s^2 = w_f = 1$ ), we have obtained  $H_0 = 70.95 \pm 0.73$  km/s/Mpc with a  $Q_{\text{DMAP}} = 3.9\sigma$ , implying that one can no longer solve the Hubble tension with this constrained ADE model, contrary to previous results [40, 41].

Let us add a few words about the  $S_8 \equiv \sigma_8 \cdot \sqrt{\Omega_m/0.3}$  tension (see *e.g.*, Ref. [116] for a review). EDE-like models are known to slightly increase the amplitude of fluctuations  $\sigma_8$  with respect to  $\Lambda$ CDM [17, 31, 117] due to an increase in  $\omega_{\text{cdm}}$  and  $n_s$ . In particular, increasing

$\omega_{\text{cdm}}$  brings forward matter-radiation equality  $a_{\text{eq}}$ , leaving more time for growing modes (that are subhorizon at  $a_{\text{eq}}$ ) to evolve in the matter era. Considering our most up-to-date dataset (*i.e.*, EFT+PanPlus+ $M_b$ ), we have obtained a Gaussian tension<sup>12</sup> on  $S_8$  of  $3.2\sigma$ ,  $3.5\sigma$  and  $3.8\sigma$  for the  $\Lambda$ CDM, ADE and axion-like EDE models, respectively. It is interesting to note that the better the model is able to resolve the Hubble tension, the higher the  $S_8$  tension. In order to resolve these two tensions simultaneously in the context of EDE cosmologies, it is therefore necessary to find a mechanism that reduces the growth of small-scale modes, as could be achieved by an interaction between EDE and DM [120].

In this paper, we have shown that the new data from Pantheon and  $SH_0ES$ , and to a lesser extent the EFTofLSS applied to the BOSS and eBOSS data, can have a decisive impact on models which aim to resolve the Hubble tension. We leave for future work the study of the impact on the Hubble tension of such an analysis applied to other early dark energy models, such as new early dark energy [19, 20], rock “n” roll dark energy [22], or early modified gravity [25, 121].

## ACKNOWLEDGMENTS

The author would like to warmly thank Vivian Poulin and Tristan L. Smith for their comments and insights throughout the project. Much of this work was carried out during a four-week visit to the *Center for Theoretical physics* (CTP) at the *Massachusetts Institute of Technology* (MIT). The author would therefore like to express his gratitude to the members of the CTP, and in particular to Tracy Slatyer, for their hospitality and kindness. These results have been made possible thanks to LUPM’s cloud computing infrastructure founded by Ocevu labex, and France-Grilles. This project has received support from the European Union’s Horizon 2020 research and innovation program under the Marie Skłodowska-Curie grant agreement No 860881-HIDDEN. This project has also received funding from the European Research Council (ERC) under the European Union’s HORIZON-ERC-2022 (Grant agreement No. 101076865).

<sup>12</sup> We use here the Gaussian metric  $(\theta_i - \theta_j)/\sqrt{\sigma_{\theta,i}^2 + \sigma_{\theta,j}^2}$ , where  $\theta_i$  and  $\sigma_{\theta,i}$  are, respectively, the mean value and the standard deviation of the parameter  $\theta$  for the dataset  $i$ . For the weak lensing determination of the  $S_8$  parameter, we use the simple weighted mean and uncertainty of  $S_8^{\text{GT}} = 0.766^{+0.020}_{-0.014}$  from the combination of KiDS-1000+dFLensS+BOSS,  $S_8 = 0.769^{+0.016}_{-0.012}$  [118], and DES-Y3,  $S_8 = 0.775^{+0.026}_{-0.024}$  [119].

## Appendix A: $M_b$ prior

In this appendix, we show explicitly, thanks to Fig 6, that the addition of the  $M_b$  prior [2] on top of the Pantheon+ likelihood is equivalent to the use of the full Pantheon+/ $SH_0$ ES likelihood as provided in Ref. [2]. Since the constraints are similar, we have chosen to show in this paper the results with the  $M_b$  prior, for the sake

of convenience, in order to determine the  $Q_{\text{DMAP}}$  values easily.

## Appendix B: $\chi^2$ table

In this appendix, we report the best-fit  $\chi^2$  per experiment for the  $\Lambda$ CDM model, the ADE model, as well as the axion-like EDE model for several combinations of data.

- 
- [1] N. Aghanim et al. (Planck), “Planck 2018 results. VI. Cosmological parameters,” *Astron. Astrophys.* **641**, A6 (2020), [Erratum: *Astron. Astrophys.* 652, C4 (2021)], arXiv:1807.06209 [astro-ph.CO].
  - [2] Adam G. Riess et al., “A Comprehensive Measurement of the Local Value of the Hubble Constant with 1 km/s/Mpc Uncertainty from the Hubble Space Telescope and the SH0ES Team,” (2021), arXiv:2112.04510 [astro-ph.CO].
  - [3] Adam G. Riess, Louise Breuval, Wenlong Yuan, Stefano Casertano, Lucas M. Macri, J. Bradley Bowers, Dan Scolnic, Tristan Cantat-Gaudin, Richard I. Anderson, and Mauricio Cruz Reyes, “Cluster Cepheids with High Precision Gaia Parallaxes, Low Zero-point Uncertainties, and Hubble Space Telescope Photometry,” *Astrophys. J.* **938**, 36 (2022), arXiv:2208.01045 [astro-ph.CO].
  - [4] Maria Giovanna Dainotti, Biagio De Simone, Tiziano Schiavone, Giovanni Montani, Enrico Rinaldi, and Gaetano Lambiase, “On the Hubble constant tension in the SNe Ia Pantheon sample,” *Astrophys. J.* **912**, 150 (2021), arXiv:2103.02117 [astro-ph.CO].
  - [5] Maria Giovanna Dainotti, Biagio De Simone, Tiziano Schiavone, Giovanni Montani, Enrico Rinaldi, Gaetano Lambiase, Malgorzata Bogdan, and Sahil Ugale, “On the Evolution of the Hubble Constant with the SNe Ia Pantheon Sample and Baryon Acoustic Oscillations: A Feasibility Study for GRB-Cosmology in 2030,” *Galaxies* **10**, 24 (2022), arXiv:2201.09848 [astro-ph.CO].
  - [6] Edvard Mortsell, Ariel Goobar, Joel Johansson, and Suhail Dhawan, “Sensitivity of the Hubble Constant Determination to Cepheid Calibration,” *Astrophys. J.* **933**, 212 (2022), arXiv:2105.11461 [astro-ph.CO].
  - [7] Edvard Mortsell, Ariel Goobar, Joel Johansson, and Suhail Dhawan, “The Hubble Tension Revisited: Additional Local Distance Ladder Uncertainties,” *Astrophys. J.* **935**, 58 (2022), arXiv:2106.09400 [astro-ph.CO].
  - [8] Brent Follin and Lloyd Knox, “Insensitivity of the distance ladder Hubble constant determination to Cepheid calibration modelling choices,” *Mon. Not. Roy. Astron. Soc.* **477**, 4534–4542 (2018), arXiv:1707.01175 [astro-ph.CO].
  - [9] Dillon Brout and Daniel Scolnic, “It’s Dust: Solving the Mysteries of the Intrinsic Scatter and Host-galaxy Dependence of Standardized Type Ia Supernova Brightnesses,” *Astrophys. J.* **909**, 26 (2021), arXiv:2004.10206 [astro-ph.CO].
  - [10] Jose Luis Bernal, Licia Verde, and Adam G. Riess, “The trouble with  $H_0$ ,” *JCAP* **1610**, 019 (2016), arXiv:1607.05617 [astro-ph.CO].
  - [11] Kevin Aylor, MacKenzie Joy, Lloyd Knox, Marius Millea, Srinivasan Raghunathan, and W. L. Kimmy Wu, “Sounds Discordant: Classical Distance Ladder &  $\Lambda$ CDM -based Determinations of the Cosmological Sound Horizon,” *Astrophys. J.* **874**, 4 (2019), arXiv:1811.00537 [astro-ph.CO].
  - [12] Lloyd Knox and Marius Millea, “Hubble constant hunter’s guide,” *Phys. Rev. D* **101**, 043533 (2020), arXiv:1908.03663 [astro-ph.CO].
  - [13] David Camarena and Valerio Marra, “On the use of the local prior on the absolute magnitude of Type Ia supernovae in cosmological inference,” *Mon. Not. Roy. Astron. Soc.* **504**, 5164–5171 (2021), arXiv:2101.08641 [astro-ph.CO].
  - [14] George Efstathiou, “To  $H_0$  or not to  $H_0$ ?” arXiv e-prints (2021), arXiv:2103.08723 [astro-ph.CO].
  - [15] Nils Schöneberg, Guillermo Franco Abellán, Andrea Pérez Sánchez, Samuel J. Witte, Vivian Poulin, and Julien Lesgourgues, “The  $H_0$  Olympics: A fair ranking of proposed models,” (2021), arXiv:2107.10291 [astro-ph.CO].
  - [16] Tanvi Karwal and Marc Kamionkowski, “Dark energy at early times, the Hubble parameter, and the string axiverse,” *Phys. Rev.* **D94**, 103523 (2016), arXiv:1608.01309 [astro-ph.CO].
  - [17] Vivian Poulin, Tristan L. Smith, Tanvi Karwal, and Marc Kamionkowski, “Early Dark Energy Can Resolve The Hubble Tension,” *Phys. Rev. Lett.* **122**, 221301 (2019), arXiv:1811.04083 [astro-ph.CO].
  - [18] Tristan L. Smith, Vivian Poulin, and Mustafa A. Amin, “Oscillating scalar fields and the Hubble tension: a resolution with novel signatures,” *Phys. Rev. D* **101**, 063523 (2020), arXiv:1908.06995 [astro-ph.CO].
  - [19] Florian Niedermann and Martin S. Sloth, “New Early Dark Energy,” (2019), arXiv:1910.10739 [astro-ph.CO].
  - [20] Florian Niedermann and Martin S. Sloth, “Resolving the Hubble Tension with New Early Dark Energy,” (2020), arXiv:2006.06686 [astro-ph.CO].
  - [21] Gen Ye and Yun-Song Piao, “Is the Hubble tension a hint of AdS phase around recombination?” *Phys. Rev. D* **101**, 083507 (2020), arXiv:2001.02451 [astro-ph.CO].
  - [22] Prateek Agrawal, Francis-Yan Cyr-Racine, David Pinner, and Lisa Randall, “Rock ‘n’ Roll Solutions to the Hubble Tension,” (2019), arXiv:1904.01016 [astro-ph.CO].

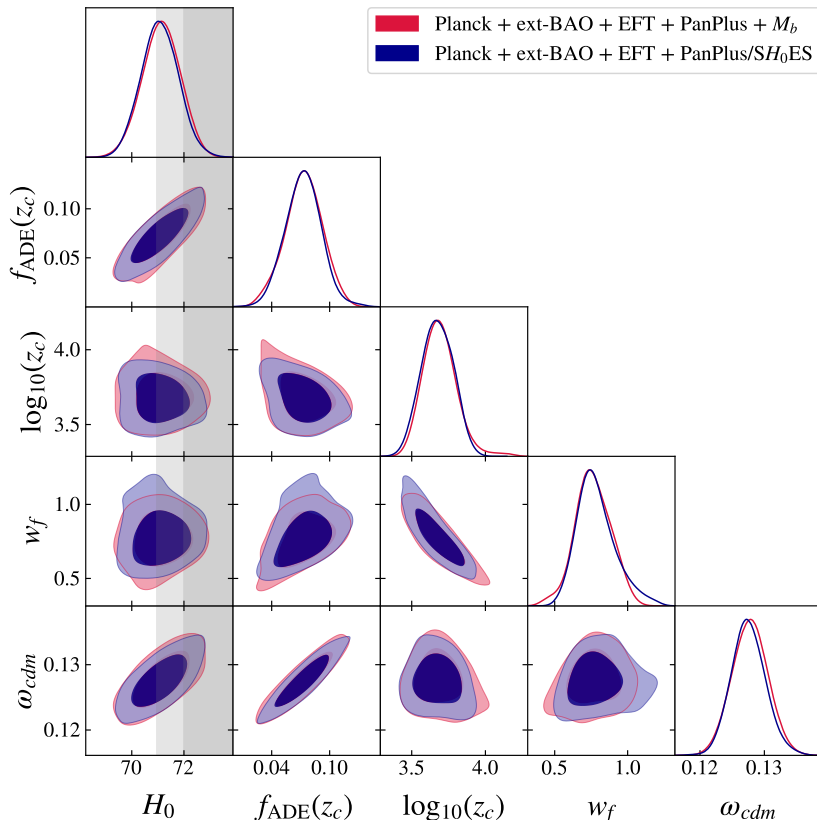


FIG. 6. 2D posterior distributions reconstructed from *Planck* + ext-BAO + EFT, either with the  $M_b$  prior on top of the Pantheon+ likelihood, or with the cross-correlation between the Pantheon+ data and the  $SH_0ES$  data (namely, the Pantheon+/ $SH_0ES$  likelihood) as provided in Ref. [2]. The gray band corresponds to the  $H_0$  constraint associated with the  $M_b$  prior, namely,  $H_0 = (73.04 \pm 1.04)$  km/s/Mpc [2].

- [23] Kim V. Berghaus and Tanvi Karwal, “Thermal Friction as a Solution to the Hubble Tension,” *Phys. Rev. D* **101**, 083537 (2020), arXiv:1911.06281 [astro-ph.CO].
- [24] Matteo Braglia, William T. Emond, Fabio Finelli, A. Emir Gumrukuoglu, and Kazuya Koyama, “Unified framework for early dark energy from  $\alpha$ -attractors,” *Phys. Rev. D* **102**, 083513 (2020), arXiv:2005.14053 [astro-ph.CO].
- [25] Matteo Braglia, Mario Ballardini, Fabio Finelli, and Kazuya Koyama, “Early modified gravity in light of the  $H_0$  tension and LSS data,” *Phys. Rev. D* **103**, 043528 (2021), arXiv:2011.12934 [astro-ph.CO].
- [26] Mark Gonzalez, Mark P. Hertzberg, and Fabrizio Rompineve, “Ultralight Scalar Decay and the Hubble Tension,” (2020), arXiv:2006.13959 [astro-ph.CO].
- [27] K. Rezazadeh, A. Ashoorioon, and D. Grin, “Cascading Dark Energy,” (2022), arXiv:2208.07631 [astro-ph.CO].
- [28] Laura Herold, Elisa G. M. Ferreira, and Eiichiro Komatsu, “New constraint on Early Dark Energy from Planck and BOSS data using the profile likelihood,” (2021), arXiv:2112.12140 [astro-ph.CO].
- [29] Adrià Gómez-Valent, “Fast test to assess the impact of marginalization in Monte Carlo analyses and its application to cosmology,” *Phys. Rev. D* **106**, 063506 (2022), arXiv:2203.16285 [astro-ph.CO].
- [30] Vivian Poulin, Tristan L. Smith, and Alexa Bartlett, “Dark Energy at early times and ACT: a larger Hubble constant without late-time priors,” (2021), arXiv:2109.06229 [astro-ph.CO].
- [31] J. Colin Hill, Evan McDonough, Michael W. Toomey, and Stephon Alexander, “Early dark energy does not restore cosmological concordance,” *Phys. Rev. D* **102**, 043507 (2020), arXiv:2003.07355 [astro-ph.CO].
- [32] Adrien La Posta, Thibaut Louis, Xavier Garrido, and J. Colin Hill, “Constraints on Pre-Recombination Early Dark Energy from SPT-3G Public Data,” (2021), arXiv:2112.10754 [astro-ph.CO].
- [33] Alexander Reeves, Laura Herold, Sunny Vagnozzi, Blake D. Sherwin, and Elisa G. M. Ferreira, “Restoring cosmological concordance with early dark energy and massive neutrinos?” *Mon. Not. Roy. Astron. Soc.* **520**, 3688–3695 (2023), arXiv:2207.01501 [astro-ph.CO].
- [34] Laura Herold and Elisa G. M. Ferreira, “Resolving the Hubble tension with early dark energy,” *Phys. Rev. D* **108**, 043513 (2023), arXiv:2210.16296 [astro-ph.CO].
- [35] Johannes R. Eskilt, Laura Herold, Eiichiro Komatsu, Kai Murai, Toshiya Namikawa, and Fumihiro Naokawa, “Constraints on Early Dark Energy from Isotropic Cosmic Birefringence,” *Phys. Rev. Lett.* **131**, 121001 (2023), arXiv:2303.15369 [astro-ph.CO].

Data	Model	$\chi^2$ tot	P18TTTEE	P18lens	ext-BAO	BOSS	eBOSS	Pan	$M_b$	PanPlus/ $SH_0ES$
BAO/ $f\sigma_8$ +Pan	$\Lambda$ CDM	3816.39	2763.03	8.87	1.38	6.15	9.88	1027.07	–	–
	ADE	3812.50	2759.48	9.14	1.30	6.55	8.92	1027.10	–	–
	EDE	3809.87	2757.41	9.70	1.64	6.30	7.89	1026.93	–	–
BAO/ $f\sigma_8$ +Pan+ $M_b$	$\Lambda$ CDM	3847.33	2765.48	9.12	1.84	5.91	9.14	1026.89	28.94	–
	ADE	3819.06	2763.73	10.09	1.77	6.95	6.32	1026.89	3.32	–
	EDE	3812.26	2759.10	9.89	1.91	6.97	6.21	1026.87	1.31	–
EFT+Pan	$\Lambda$ CDM	4020.07	2762.14	8.87	1.25	160.20	60.44	1027.17	–	–
	ADE	4018.67	2761.21	8.99	1.40	159.63	60.39	1027.06	–	–
	EDE	4017.09	2759.20	9.29	1.60	159.54	60.51	1026.95	–	–
EFT+Pan+ $M_b$	$\Lambda$ CDM	4051.76	2764.81	9.13	1.78	158.30	61.16	1026.90	29.61	–
	ADE	4026.87	2763.76	9.62	2.11	159.94	60.26	1026.86	4.33	–
	EDE	4022.83	2758.51	9.60	1.99	160.36	61.64	1026.87	3.86	–
EFT+PanPlus	$\Lambda$ CDM	4404.28	2762.12	8.78	1.20	160.44	60.43	1411.31	–	–
	cADE	4404.07	2761.57	8.86	1.20	160.68	60.46	1411.31	–	–
	ADE	4402.96	2760.49	8.89	1.21	160.78	60.23	1411.36	–	–
	$c_s^2$ ADE	4402.93	2760.47	8.90	1.21	160.76	60.23	1411.37	–	–
	EDE	4402.54	2758.74	9.02	1.38	160.38	61.21	1411.82	–	–
EFT+PanPlus+ $M_b$	$\Lambda$ CDM	4443.78	2766.95	9.69	1.95	158.36	60.63	1413.17	33.02	–
	cADE	4419.67	2766.20	9.67	1.92	160.68	61.17	1413.27	6.76	–
	ADE	4415.94	2763.42	9.82	1.81	160.52	60.95	1412.99	6.42	–
	$c_s^2$ ADE	4415.89	2763.16	9.82	1.77	160.58	60.96	1412.91	6.70	–
	EDE	4408.67	2759.71	10.05	1.96	159.64	60.24	1413.35	3.72	–
EFT+PanPlus/ $SH_0ES$	$\Lambda$ CDM	4318.12	2767.42	9.24	2.20	158.01	60.39	–	–	1320.85
	ADE	4292.12	2763.74	9.77	1.94	160.31	60.20	–	–	1296.17

TABLE III. Table of best-fit  $\chi^2$  of the different models considered in this work for various combinations of likelihood. All datasets include *Planck* + ext-BAO data. Note that the columns “BOSS” and “eBOSS” refer either to the BAO/ $f\sigma_8$  analysis or to the EFT full-shape analysis. Similarly, the column “Pan” refers to either Pantheon data or Pantheon+ data. Finally, “PanPlus/ $SH_0ES$ ” corresponds to the full Pantheon+/ $SH_0ES$  likelihood as provided in Ref. [2].

- [36] Riccardo Murgia, Guillermo F. Abellán, and Vivian Poulin, “Early dark energy resolution to the Hubble tension in light of weak lensing surveys and lensing anomalies,” *Phys. Rev. D* **103**, 063502 (2021), arXiv:2009.10733 [astro-ph.CO].
- [37] Samuel Goldstein, J. Colin Hill, Vid Iršič, and Blake D. Sherwin, “Canonical Hubble-Tension-Resolving Early Dark Energy Cosmologies Are Inconsistent with the Lyman- $\alpha$  Forest,” *Phys. Rev. Lett.* **131**, 201001 (2023), arXiv:2303.00746 [astro-ph.CO].
- [38] Vivian Poulin, Tristan L. Smith, and Tanvi Karwal, “The Ups and Downs of Early Dark Energy solutions to the Hubble tension: a review of models, hints and constraints circa 2023,” (2023), arXiv:2302.09032 [astro-ph.CO].
- [39] Eleonora Di Valentino, Olga Mena, Supriya Pan, Luca Visinelli, Weiqiang Yang, Alessandro Melchiorri, David F. Mota, Adam G. Riess, and Joseph Silk, “In the realm of the Hubble tension—a review of solutions,” *Class. Quant. Grav.* **38**, 153001 (2021), arXiv:2103.01183 [astro-ph.CO].
- [40] Meng-Xiang Lin, Giampaolo Benevento, Wayne Hu, and Marco Raveri, “Acoustic Dark Energy: Potential Conversion of the Hubble Tension,” *Phys. Rev.* **D100**, 063542 (2019), arXiv:1905.12618 [astro-ph.CO].
- [41] Meng-Xiang Lin, Wayne Hu, and Marco Raveri, “Testing  $H_0$  in Acoustic Dark Energy with *Planck* and ACT Polarization,” *Phys. Rev. D* **102**, 123523 (2020), arXiv:2009.08974 [astro-ph.CO].
- [42] Shadab Alam et al. (BOSS), “The clustering of galaxies in the completed SDSS-III Baryon Oscillation Spectroscopic Survey: cosmological analysis of the DR12 galaxy sample,” *Mon. Not. Roy. Astron. Soc.* **470**, 2617–2652 (2017), arXiv:1607.03155 [astro-ph.CO].
- [43] Shadab Alam et al. (eBOSS), “Completed SDSS-IV extended Baryon Oscillation Spectroscopic Survey: Cosmological implications from two decades of spectroscopic surveys at the Apache Point Observatory,” *Phys. Rev. D* **103**, 083533 (2021), arXiv:2007.08991 [astro-ph.CO].
- [44] Dillon Brout et al., “The Pantheon+ Analysis: Cosmological Constraints,” (2022), arXiv:2202.04077 [astro-ph.CO].
- [45] John Joseph M. Carrasco, Mark P. Hertzberg, and Leonardo Senatore, “The Effective Field Theory of Cosmological Large Scale Structures,” *JHEP* **09**, 082 (2012), arXiv:1206.2926 [astro-ph.CO].
- [46] Daniel Baumann, Alberto Nicolis, Leonardo Senatore, and Matias Zaldarriaga, “Cosmological Non-Linearities as an Effective Fluid,” *JCAP* **07**, 051 (2012), arXiv:1004.2488 [astro-ph.CO].
- [47] Rafael A. Porto, Leonardo Senatore, and Matias Zaldarriaga, “The Lagrangian-space Effective Field Theory of Large Scale Structures,” *JCAP* **05**, 022 (2014), arXiv:1311.2168 [astro-ph.CO].

- [48] Enrico Pajer and Matias Zaldarriaga, “On the Renormalization of the Effective Field Theory of Large Scale Structures,” *JCAP* **08**, 037 (2013), arXiv:1301.7182 [astro-ph.CO].
- [49] Ali Akbar Abolhasani, Mehrdad Mirbabayi, and Enrico Pajer, “Systematic Renormalization of the Effective Theory of Large Scale Structure,” *JCAP* **05**, 063 (2016), arXiv:1509.07886 [hep-th].
- [50] Leonardo Senatore and Matias Zaldarriaga, “Redshift Space Distortions in the Effective Field Theory of Large Scale Structures,” (2014), arXiv:1409.1225 [astro-ph.CO].
- [51] Tobias Baldauf, Mehrdad Mirbabayi, Marko Simonović, and Matias Zaldarriaga, “Equivalence Principle and the Baryon Acoustic Peak,” *Phys. Rev. D* **92**, 043514 (2015), arXiv:1504.04366 [astro-ph.CO].
- [52] Leonardo Senatore and Matias Zaldarriaga, “The IR-resummed Effective Field Theory of Large Scale Structures,” *JCAP* **02**, 013 (2015), arXiv:1404.5954 [astro-ph.CO].
- [53] Leonardo Senatore and Gabriele Trevisan, “On the IR-Resummation in the EFTofLSS,” *JCAP* **05**, 019 (2018), arXiv:1710.02178 [astro-ph.CO].
- [54] Matthew Lewandowski and Leonardo Senatore, “An analytic implementation of the IR-resummation for the BAO peak,” *JCAP* **03**, 018 (2020), arXiv:1810.11855 [astro-ph.CO].
- [55] Diego Blas, Mathias Garny, Mikhail M. Ivanov, and Sergey Sibiryakov, “Time-Sliced Perturbation Theory II: Baryon Acoustic Oscillations and Infrared Resummation,” *JCAP* **07**, 028 (2016), arXiv:1605.02149 [astro-ph.CO].
- [56] John Joseph M. Carrasco, Simon Foreman, Daniel Green, and Leonardo Senatore, “The 2-loop matter power spectrum and the IR-safe integrand,” *JCAP* **07**, 056 (2014), arXiv:1304.4946 [astro-ph.CO].
- [57] John Joseph M. Carrasco, Simon Foreman, Daniel Green, and Leonardo Senatore, “The Effective Field Theory of Large Scale Structures at Two Loops,” *JCAP* **07**, 057 (2014), arXiv:1310.0464 [astro-ph.CO].
- [58] Leonardo Senatore, “Bias in the Effective Field Theory of Large Scale Structures,” *JCAP* **11**, 007 (2015), arXiv:1406.7843 [astro-ph.CO].
- [59] Mehrdad Mirbabayi, Fabian Schmidt, and Matias Zaldarriaga, “Biased Tracers and Time Evolution,” *JCAP* **07**, 030 (2015), arXiv:1412.5169 [astro-ph.CO].
- [60] Raul Angulo, Matteo Fasiello, Leonardo Senatore, and Zvonimir Vlah, “On the Statistics of Biased Tracers in the Effective Field Theory of Large Scale Structures,” *JCAP* **1509**, 029 (2015), arXiv:1503.08826 [astro-ph.CO].
- [61] Tomohiro Fujita, Valentin Mauerhofer, Leonardo Senatore, Zvonimir Vlah, and Raul Angulo, “Very Massive Tracers and Higher Derivative Biases,” *JCAP* **01**, 009 (2020), arXiv:1609.00717 [astro-ph.CO].
- [62] Ashley Perko, Leonardo Senatore, Elise Jennings, and Risa H. Wechsler, “Biased Tracers in Redshift Space in the EFT of Large-Scale Structure,” (2016), arXiv:1610.09321 [astro-ph.CO].
- [63] Ethan O. Nadler, Ashley Perko, and Leonardo Senatore, “On the Bispectra of Very Massive Tracers in the Effective Field Theory of Large-Scale Structure,” *JCAP* **02**, 058 (2018), arXiv:1710.10308 [astro-ph.CO].
- [64] Guido D’Amico, Jérôme Gleyzes, Nickolas Kokron, Katarina Markovic, Leonardo Senatore, Pierre Zhang, Florian Beutler, and Héctor Gil-Marín, “The Cosmological Analysis of the SDSS/BOSS data from the Effective Field Theory of Large-Scale Structure,” *JCAP* **05**, 005 (2020), arXiv:1909.05271 [astro-ph.CO].
- [65] Théo Simon, Pierre Zhang, and Vivian Poulin, “Cosmological inference from the EFTofLSS: the eBOSS QSO full-shape analysis,” *JCAP* **07**, 041 (2023), arXiv:2210.14931 [astro-ph.CO].
- [66] Mikhail M. Ivanov, Marko Simonović, and Matias Zaldarriaga, “Cosmological Parameters from the BOSS Galaxy Power Spectrum,” *JCAP* **05**, 042 (2020), arXiv:1909.05277 [astro-ph.CO].
- [67] Thomas Colas, Guido D’Amico, Leonardo Senatore, Pierre Zhang, and Florian Beutler, “Efficient Cosmological Analysis of the SDSS/BOSS data from the Effective Field Theory of Large-Scale Structure,” *JCAP* **06**, 001 (2020), arXiv:1909.07951 [astro-ph.CO].
- [68] Guido D’Amico, Leonardo Senatore, and Pierre Zhang, “Limits on  $w$ CDM from the EFTofLSS with the PyBird code,” (2020), arXiv:2003.07956 [astro-ph.CO].
- [69] Guido D’Amico, Yaniv Donath, Leonardo Senatore, and Pierre Zhang, “Limits on Clustering and Smooth Quintessence from the EFTofLSS,” (2020), arXiv:2012.07554 [astro-ph.CO].
- [70] Théo Simon, Guillermo Franco Abellán, Peizhi Du, Vivian Poulin, and Yuhsin Tsai, “Constraining decaying dark matter with BOSS data and the effective field theory of large-scale structures,” *Phys. Rev. D* **106**, 023516 (2022), arXiv:2203.07440 [astro-ph.CO].
- [71] Théo Simon, Pierre Zhang, Vivian Poulin, and Tristan L. Smith, “Consistency of effective field theory analyses of the BOSS power spectrum,” *Phys. Rev. D* **107**, 123530 (2023), arXiv:2208.05929 [astro-ph.CO].
- [72] Shi-Fan Chen, Zvonimir Vlah, and Martin White, “A new analysis of galaxy 2-point functions in the BOSS survey, including full-shape information and post-reconstruction BAO,” *JCAP* **02**, 008 (2022), arXiv:2110.05530 [astro-ph.CO].
- [73] Pierre Zhang, Guido D’Amico, Leonardo Senatore, Cheng Zhao, and Yifu Cai, “BOSS Correlation Function analysis from the Effective Field Theory of Large-Scale Structure,” *JCAP* **02**, 036 (2022), arXiv:2110.07539 [astro-ph.CO].
- [74] Oliver H. E. Philcox and Mikhail M. Ivanov, “BOSS DR12 full-shape cosmology:  $\Lambda$ CDM constraints from the large-scale galaxy power spectrum and bispectrum monopole,” *Phys. Rev. D* **105**, 043517 (2022), arXiv:2112.04515 [astro-ph.CO].
- [75] Suresh Kumar, Rafael C. Nunes, and Priya Yadav, “Updating non-standard neutrinos properties with Planck-CMB data and full-shape analysis of BOSS and eBOSS galaxies,” *JCAP* **09**, 060 (2022), arXiv:2205.04292 [astro-ph.CO].
- [76] Rafael C. Nunes, Sunny Vagnozzi, Suresh Kumar, Eleonora Di Valentino, and Olga Mena, “New tests of dark sector interactions from the full-shape galaxy power spectrum,” *Phys. Rev. D* **105**, 123506 (2022), arXiv:2203.08093 [astro-ph.CO].
- [77] Alex Laguë, J. Richard Bond, Renée Hložek, Keir K. Rogers, David J. E. Marsh, and Daniel Grin, “Constraining Ultralight Axions with Galaxy Surveys,” (2021), arXiv:2104.07802 [astro-ph.CO].



- [78] Oliver H.E. Philcox, Blake D. Sherwin, Gerrit S. Farren, and Eric J. Baxter, “Determining the Hubble Constant without the Sound Horizon: Measurements from Galaxy Surveys,” (2020), arXiv:2008.08084 [astro-ph.CO].
- [79] Tristan L. Smith, Vivian Poulin, and Théo Simon, “Assessing the robustness of sound horizon-free determinations of the Hubble constant,” (2022), arXiv:2208.12992 [astro-ph.CO].
- [80] Chiara Moretti, Maria Tsedrik, Pedro Carrilho, and Alkistis Pourtsidou, “Modified gravity and massive neutrinos: constraints from the full shape analysis of BOSS galaxies and forecasts for Stage IV surveys,” (2023), arXiv:2306.09275 [astro-ph.CO].
- [81] Henrique Rubira, Asmaa Mazoun, and Mathias Garny, “Full-shape BOSS constraints on dark matter interacting with dark radiation and lifting the S8 tension,” JCAP **01**, 034 (2023), arXiv:2209.03974 [astro-ph.CO].
- [82] Nils Schöneberg, Guillermo Franco Abellán, Théo Simon, Alexa Bartlett, Yashvi Patel, and Tristan L. Smith, “The weak, the strong and the ugly – A comparative analysis of interacting stepped dark radiation,” (2023), arXiv:2306.12469 [astro-ph.CO].
- [83] Emil Brinch Holm, Laura Herold, Théo Simon, Elisa G. M. Ferreira, Steen Hannestad, Vivian Poulin, and Thomas Tram, “Bayesian and frequentist investigation of prior effects in EFTofLSS analyses of full-shape BOSS and eBOSS data,” (2023), arXiv:2309.04468 [astro-ph.CO].
- [84] Théo Simon, Pierre Zhang, Vivian Poulin, and Tristan L. Smith, “Updated constraints from the effective field theory analysis of the BOSS power spectrum on early dark energy,” Phys. Rev. D **107**, 063505 (2023), arXiv:2208.05930 [astro-ph.CO].
- [85] Guido D’Amico, Leonardo Senatore, Pierre Zhang, and Henry Zheng, “The Hubble Tension in Light of the Full-Shape Analysis of Large-Scale Structure Data,” (2020), arXiv:2006.12420 [astro-ph.CO].
- [86] Tristan L. Smith, Vivian Poulin, José Luis Bernal, Kimberley K. Boddy, Marc Kamionkowski, and Riccardo Murgia, “Early dark energy is not excluded by current large-scale structure data,” Phys. Rev. D **103**, 123542 (2021), arXiv:2009.10740 [astro-ph.CO].
- [87] Mikhail M. Ivanov, Evan McDonough, J. Colin Hill, Marko Simonović, Michael W. Toomey, Stephon Alexander, and Matias Zaldarriaga, “Constraining Early Dark Energy with Large-Scale Structure,” Phys. Rev. D **102**, 103502 (2020), arXiv:2006.11235 [astro-ph.CO].
- [88] Alain Blanchard, Jean-Yves Héloret, Stéphan Ilić, Brahim Lamine, and Isaac Tutusaus, “ $\Lambda$ CDM is alive and well,” (2022), arXiv:2205.05017 [astro-ph.CO].
- [89] Vivian Poulin, Tristan L. Smith, Daniel Grin, Tanvi Karwal, and Marc Kamionkowski, “Cosmological implications of ultralight axionlike fields,” Phys. Rev. D **98**, 083525 (2018), arXiv:1806.10608 [astro-ph.CO].
- [90] C. Armendariz-Picon, Viatcheslav F. Mukhanov, and Paul J. Steinhardt, “Essentials of k essence,” Phys. Rev. D **63**, 103510 (2001), arXiv:astro-ph/0006373.
- [91] Christopher Gordon and Wayne Hu, “A Low CMB quadrupole from dark energy isocurvature perturbations,” Phys. Rev. D **70**, 083003 (2004), arXiv:astro-ph/0406496.
- [92] Adrià Gómez-Valent, Ziyang Zheng, Luca Amendola, Valeria Pettorino, and Christof Wetterich, “Early dark energy in the pre- and postrecombination epochs,” Phys. Rev. D **104**, 083536 (2021), arXiv:2107.11065 [astro-ph.CO].
- [93] Michael S. Turner, “Coherent scalar-field oscillations in an expanding universe,” Phys. Rev. D **28**, 1243–1247 (1983).
- [94] Chung-Pei Ma and Edmund Bertschinger, “Cosmological perturbation theory in the synchronous and conformal Newtonian gauges,” Astrophys. J. **455**, 7–25 (1995), arXiv:astro-ph/9506072.
- [95] Thejs Brinckmann and Julien Lesgourgues, “MontePython 3: boosted MCMC sampler and other features,” (2018), arXiv:1804.07261 [astro-ph.CO].
- [96] Benjamin Audren, Julien Lesgourgues, Karim Benabed, and Simon Prunet, “Conservative Constraints on Early Cosmology: an illustration of the Monte Python cosmological parameter inference code,” JCAP **1302**, 001 (2013), arXiv:1210.7183 [astro-ph.CO].
- [97] Julien Lesgourgues, “The Cosmic Linear Anisotropy Solving System (CLASS) I: Overview,” (2011), arXiv:1104.2932 [astro-ph.IM].
- [98] Diego Blas, Julien Lesgourgues, and Thomas Tram, “The Cosmic Linear Anisotropy Solving System (CLASS) II: Approximation schemes,” JCAP **1107**, 034 (2011), arXiv:1104.2933 [astro-ph.CO].
- [99] N. Aghanim et al. (Planck), “Planck 2018 results. V. CMB power spectra and likelihoods,” Astron. Astrophys. **641**, A5 (2020), arXiv:1907.12875 [astro-ph.CO].
- [100] N. Aghanim et al. (Planck), “Planck 2018 results. VIII. Gravitational lensing,” Astron. Astrophys. **641**, A8 (2020), arXiv:1807.06210 [astro-ph.CO].
- [101] Florian Beutler, Chris Blake, Matthew Colless, D. Heath Jones, Lister Staveley-Smith, Lachlan Campbell, Quentin Parker, Will Saunders, and Fred Watson, “The 6dF Galaxy Survey: Baryon Acoustic Oscillations and the Local Hubble Constant,” Mon. Not. Roy. Astron. Soc. **416**, 3017–3032 (2011), arXiv:1106.3366 [astro-ph.CO].
- [102] Ashley J. Ross, Lado Samushia, Cullan Howlett, Will J. Percival, Angela Burden, and Marc Manera, “The clustering of the SDSS DR7 main Galaxy sample – I. A 4 per cent distance measure at  $z = 0.15$ ,” Mon. Not. Roy. Astron. Soc. **449**, 835–847 (2015), arXiv:1409.3242 [astro-ph.CO].
- [103] Héctor Gil-Marín et al., “The clustering of galaxies in the SDSS-III Baryon Oscillation Spectroscopic Survey: BAO measurement from the LOS-dependent power spectrum of DR12 BOSS galaxies,” Mon. Not. Roy. Astron. Soc. **460**, 4210–4219 (2016), arXiv:1509.06373 [astro-ph.CO].
- [104] Francisco-Shu Kitaura et al., “The clustering of galaxies in the SDSS-III Baryon Oscillation Spectroscopic Survey: mock galaxy catalogues for the BOSS Final Data Release,” Mon. Not. Roy. Astron. Soc. **456**, 4156–4173 (2016), arXiv:1509.06400 [astro-ph.CO].
- [105] Beth Reid et al., “SDSS-III Baryon Oscillation Spectroscopic Survey Data Release 12: galaxy target selection and large scale structure catalogues,” Mon. Not. Roy. Astron. Soc. **455**, 1553–1573 (2016), arXiv:1509.06529 [astro-ph.CO].
- [106] Takahiro Nishimichi, Guido D’Amico, Mikhail M. Ivanov, Leonardo Senatore, Marko Simonović, Masahiro Takada, Matias Zaldarriaga, and Pierre Zhang, “Blinded challenge for precision cosmology with large-

- scale structure: results from effective field theory for the redshift-space galaxy power spectrum,” *Phys. Rev. D* **102**, 123541 (2020), arXiv:2003.08277 [astro-ph.CO].
- [107] Ashley J. Ross et al., “The Completed SDSS-IV extended Baryon Oscillation Spectroscopic Survey: Large-scale structure catalogues for cosmological analysis,” *Mon. Not. Roy. Astron. Soc.* **498**, 2354–2371 (2020), arXiv:2007.09000 [astro-ph.CO].
- [108] Chia-Hsun Chuang, Francisco-Shu Kitaura, Francisco Prada, Cheng Zhao, and Gustavo Yepes, “EZmocks: extending the Zel’dovich approximation to generate mock galaxy catalogues with accurate clustering statistics,” *Mon. Not. Roy. Astron. Soc.* **446**, 2621–2628 (2015), arXiv:1409.1124 [astro-ph.CO].
- [109] Florian Beutler and Patrick McDonald, “Unified galaxy power spectrum measurements from 6dFGS, BOSS, and eBOSS,” *JCAP* **11**, 031 (2021), arXiv:2106.06324 [astro-ph.CO].
- [110] Jiamin Hou et al., “The Completed SDSS-IV extended Baryon Oscillation Spectroscopic Survey: BAO and RSD measurements from anisotropic clustering analysis of the Quasar Sample in configuration space between redshift 0.8 and 2.2,” *Mon. Not. Roy. Astron. Soc.* **500**, 1201–1221 (2020), arXiv:2007.08998 [astro-ph.CO].
- [111] D. M. Scolnic et al., “The Complete Light-curve Sample of Spectroscopically Confirmed SNe Ia from Pan-STARRS1 and Cosmological Constraints from the Combined Pantheon Sample,” *Astrophys. J.* **859**, 101 (2018), arXiv:1710.00845 [astro-ph.CO].
- [112] Alexander Mead, Samuel Brieden, Tilman Tröster, and Catherine Heymans, “HMcode-2020: Improved modelling of non-linear cosmological power spectra with baryonic feedback,” (2020), 10.1093/mnras/stab082, arXiv:2009.01858 [astro-ph.CO].
- [113] Antony Lewis, “GetDist: a Python package for analysing Monte Carlo samples,” (2019), arXiv:1910.13970 [astro-ph.IM].
- [114] Marco Raveri and Wayne Hu, “Concordance and discordance in cosmology,” *Phys. Rev. D* **99**, 043506 (2019), arXiv:1806.04649 [astro-ph.CO].
- [115] Adam G. Riess, Stefano Casertano, Wenlong Yuan, Lucas M. Macri, and Dan Scolnic, “Large Magellanic Cloud Cepheid Standards Provide a 1% Foundation for the Determination of the Hubble Constant and Stronger Evidence for Physics beyond  $\Lambda$ CDM,” *Astrophys. J.* **876**, 85 (2019), arXiv:1903.07603 [astro-ph.CO].
- [116] Elcio Abdalla et al., “Cosmology intertwined: A review of the particle physics, astrophysics, and cosmology associated with the cosmological tensions and anomalies,” *JHEAp* **34**, 49–211 (2022), arXiv:2203.06142 [astro-ph.CO].
- [117] Sunny Vagnozzi, “Consistency tests of  $\Lambda$ CDM from the early integrated Sachs-Wolfe effect: Implications for early-time new physics and the Hubble tension,” *Phys. Rev. D* **104**, 063524 (2021), arXiv:2105.10425 [astro-ph.CO].
- [118] Catherine Heymans et al., “KiDS-1000 Cosmology: Multi-probe weak gravitational lensing and spectroscopic galaxy clustering constraints,” *Astron. Astrophys.* **646**, A140 (2021), arXiv:2007.15632 [astro-ph.CO].
- [119] T. M. C. Abbott et al. (DES), “Dark Energy Survey Year 3 Results: Cosmological Constraints from Galaxy Clustering and Weak Lensing,” (2021), arXiv:2105.13549 [astro-ph.CO].
- [120] Gang Liu, Jiaye Gao, Yufen Han, Yuhao Mu, and Lixin Xu, “Mitigating Cosmological Tensions via Momentum-Coupled Dark Sector Model,” (2023), arXiv:2310.09798 [astro-ph.CO].
- [121] Guillermo Franco Abellán, Matteo Braglia, Mario Ballardini, Fabio Finelli, and Vivian Poulin, “Probing Early Modification of Gravity with Planck, ACT and SPT,” (2023), arXiv:2308.12345 [astro-ph.CO].